HEAVY PHOTON SEARCH

TEST RUN

A Proposal to Search for Massive Photons at Jefferson Laboratory

February 18, 2010

Authors

A. Grillo, V. Fadeyev
University of California, Santa Cruz, CA 95064

M. Ungaro
University of Connecticut, Department of Physics, Storrs, CT 06269

W. Cooper
Fermi National Accelerator Laboratory, Batavia, IL 60510-5011

A. Micherdzinska
The George Washington University, Department of Physics,Washington, DC 20052

G. Ron
Hebrew University of Jerusalem, Jerusalem, Israel

M. Battaglieri, R. De Vita
INFN, Sezione di Genova, 16146 Genova, Italy

M. Holtrop (Co-Spokesperson), K. Slifer, S. K. Phillips, E. Ebrahim
University of New Hampshire, Department of Physics, Durham, NH 03824

M. Khandaker, C. Salgado
Norfolk State University, Department of Physics, Norfolk, VA 23504

S. Bueltmann, L. Weinstein
Old Dominion University, Department of Physics, Norfolk, VA 23529

A. Fradi, B. Guegan, M. Guidal, S. Niccolai, S. Pisano, E. Rauly, P. Rosier and D. Sokhan
Institut de Physique Nucleaire d'Orsay, 91405 Orsay, France

P. Schuster, N. Toro
Perimeter Institute, Ontario, Canada N2L 2Y5

P. Stoler, A. Kubarovsky
Rensselaer Polytechnic Institute, Department of Physics, Troy, NY 12181

R. Essig, C. Field, M. Graham, G. Haller, R. Herbst, J. Jaros (Co-Spokesperson), C. Kenney, T. Maruyama, K. Moffeit, T. Nelson, H. Neal, A. Odian, M. Oriunno, R. Partridge, S. Uemura, D. Walz
SLAC National Accelerator Laboratory, Menlo Park, CA 94025

S. Boyarinov, V. Burkert, A. Deur, H. Egiyan, L. Elouadrhiri, A. Freyberger, F.-X. Girod, V. Kubarovsky, Y. Sharabian, S. Stepanyan (Co-Spokesperson), B. Wojtsekhowski
Thomas Jefferson National Accelerator Facility, Newport News, VA 23606

K. Griffioen
The College of William and Mary, Department of Physics, Williamsburg, VA 23185

N. Dashyan, N. Gevorgyan, R. Paremuzyan, H. Voskanyan
Yerevan Physics Institute, 375036 Yerevan, Armenia

Abstract

The Heavy Photon Search Test Run is the first stage of the Heavy Photon Search experiment, which will search for new heavy vector boson(s), aka "heavy photons", at Jefferson Laboratory. The HPS Test Run was approved by the Jefferson Laboratory PAC on January 14, 2011, and is seeking funding from DOE HEP in this proposal. The HPS experiment proper will utilize a compact, large acceptance forward spectrometer, silicon microstrip vertex tracker, and $PbWO_4$ electromagnetic calorimeter to search for electro-produced heavy photons decaying to e^+e^- in the mass range of 20 to 1000 MeV/c^2 . Heavy photons would be visible as narrow resonances above the copious QED trident background, and by detection of their secondary decay vertices downstream of the target. High luminosities are required to search for heavy photons because of their weak couplings to electrons and the prolific backgrounds. HPS achieves great sensitivity by exploiting CEBAF's 100% duty cycle, high luminosities, and 40 MHz continuous readout, and by placing silicon microstrip detectors and the electromagnetic calorimeter used for triggering in close proximity to a hot electron beam. The purpose of the HPS Test Run is to verify detailed full Monte Carlo simulations that microstrip occupancies and ECal trigger rates are manageable in this environment with a simplified version of the HPS apparatus. The Test Run will also demonstrate that the tracker and ECal sensors and readout are operable, and that the data acquisition can run at very high rates. The Test Run apparatus is capable of high rate triggering, full track finding, momentum measurement, and vertexing, so it is capable of demonstrating the physics capability of the full HPS. In particular, the Test Run apparatus is capable of extending the search for heavy photons into virgin territory with even modest run times. The HPS Test Run experiment is ready to proceed to full engineering design, fabrication, assembly and test over the remainder of 2011, and to be ready for full integration and installation by March, 2012. A one month test run, including time for installation, commissioning, and a week of data taking, will fulfill the HPS Test Run goals.

Table of Contents

1 Introduction

This proposal seeks funding for the first stage of the Heavy Photon Search Experiment which was approved by the Thomas Jefferson National Accelerator Facility's Program Advisory Committee on January 14, 2011. PAC37 reviewed the scientific motivations for and the technical feasibility of HPS, and approved Stage I of the HPS proposal, the HPS Test Run, and urged it be scheduled before the end of 6 GeV running. They also granted approval for Stage II, the full HPS experiment, contingent on the success of the test run. Ideally, given the topical nature of heavy photon searches, Stage I of the proposal would run before the planned CEBAF shut down in the Summer of 2012, when its energy will be upgraded from 6 GeV to 12 GeV. The planned upgrade is scheduled to be completed by the end of 2013, with commissioning and some first running in 2014 and the resumption of a full experimental schedule in 2015. The full HPS run is planned for the 12 GeV era of CEBAF.

The highest priority goal of the HPS Test run is to validate the fundamental assumptions behind the design of the full HPS experiment and thereby prepare the foundation for full HPS approval. A critical design feature of the HPS is the placement of silicon microstrip detectors in close proximity to an intense electron beam and tracking and vertexing in the resultant high occupancy environment. The experiment is also dependent on placing an electromagnetic calorimeter just downstream of the tracking detectors, also in close proximity to the beam, and triggering on candidate e+e- pairs with good acceptance and efficiency and manageable rates. Measurements of tracker occupancies and trigger rates will allow us to understand the projected performance of the full experiment. Confirming that occupancies and trigger rates are manageable, which has been demonstrated in full Monte Carlo simulation, is our highest priority goal.

In order to reach this goal, the following must be accomplished. First, we must assemble the appropriate beamline, a magnet chicane, vacuum chambers, and beam diagnostics, to measure the beam sizes, halo, and stability required to measure occupancies and trigger rates. The CEBAF beam quality has been well-measured and is known to satisfy HPS experimental requirements, but, practice controlling and monitoring the incident electron beam is prerequisite for successful HPS operations. Second, we must instrument a silicon tracker/vertexer capable of making the occupancy measurements. We must produce working silicon sensors, front end readout, and DAQ capable of making the occupancy measurements, and capable of the high rate data acquisition needed for HPS. Third, we must implement an electromagnetic calorimeter based on existing $PbWO_4$ crystals and its readout and high speed DAQ, and construct a suitable temperature-controlled enclosure and the vacuum chamber which allows the crystals to be placed in close proximity to the beam.

Secondary objectives for the HPS Test Run can be pursued when the apparatus is commissioned and useful running conditions are established. It should be straightforward to record random events in the tracker and provide samples of tracks in the SVT. Offline analysis can then

determine tracker alignment, track finding efficiency, sensor efficiency and noise, and ultimately momentum and vertex resolution. Stable operating conditions and a successfully operating Ecal DAQ will enable commissioning of the trigger electronics. Assuming successful operation of the above-mentioned items, implemention of full rate, triggered data acquisition will be next and with it the possibility of triggering on e^+e^- pairs. This entire effort will enable tremendous strides toward our long term goal of preparing a fully operational HPS experiment.

The HPS Test Run apparatus has the potential to extend the search for a heavy photon into a virgin domain of heavy photon masses and couplings. This region is favored by ascribing the present 3.5 sigma discrepancy between the measured and predicted value for the muon's anomalous magnetic moment to the effects of a heavy photon.

The physics which motivates the HPS Test Run is exactly that which motivates the full HPS, and is discussed in detail in the HPS proposal [1]. Briefly, HPS is searching for new heavy vector boson(s), aka "heavy photons" or "dark photons" or "hidden sector photons", in the mass range of 20 MeV/c^2 to 1000 MeV/c^2. Heavy photons mix with the Standard Model photon through kinetic mixing, which induces their weak coupling to electrons, εe, where $\varepsilon \sim 10^{-3}$. Heavy photons in this mass/coupling range are expected on very general theoretical grounds, and also motivated by recent astrophysical evidence suggesting they might mediate dark matter annihilations and/or dark matter interactions with ordinary matter. Since they couple to electrons, heavy photons are radiated in electron scattering and can subsequently decay into narrow e^+e^- resonances which can be observed above the copious QED trident background. For suitably small couplings, heavy photons travel detectable distances before decaying, providing a second signature. The HPS experiment exploits both of these signatures to search for heavy photons over a wide range of couplings, $\varepsilon^2 > 10^{-10}$, and masses.

Existing constraints on heavy photon masses and couplings come from axion searches, the anomalous magnetic moments of the muon and electron, and direct searches for heavy photons in the B factory data and in recent electroproduction experiments conducted at Jefferson Lab and Mainz [2]. These constraints and the reach of the full Heavy Photon Search (HPS) experiment are shown in Figure 1.1. The potential reach of the HPS Test Run is also indicated. Roughly speaking, heavy photons are allowed below a coupling strength of few x 10^{-3} and throughout the mass range of 20-1000 MeV/c^2. As indicated in the figure, the full HPS experiment will simultaneously explore two large regions of this parameter space. One HPS search region focuses on a wide range of heavy photon masses and moderate couplings with a traditional bump-hunt search, much of which other experiments plan to probe as well. The other region is unique, and utilizes both invariant mass and separated decay vertex information to provide unparalleled sensitivity to small couplings over the mass range 20-250 MeV/c^2.

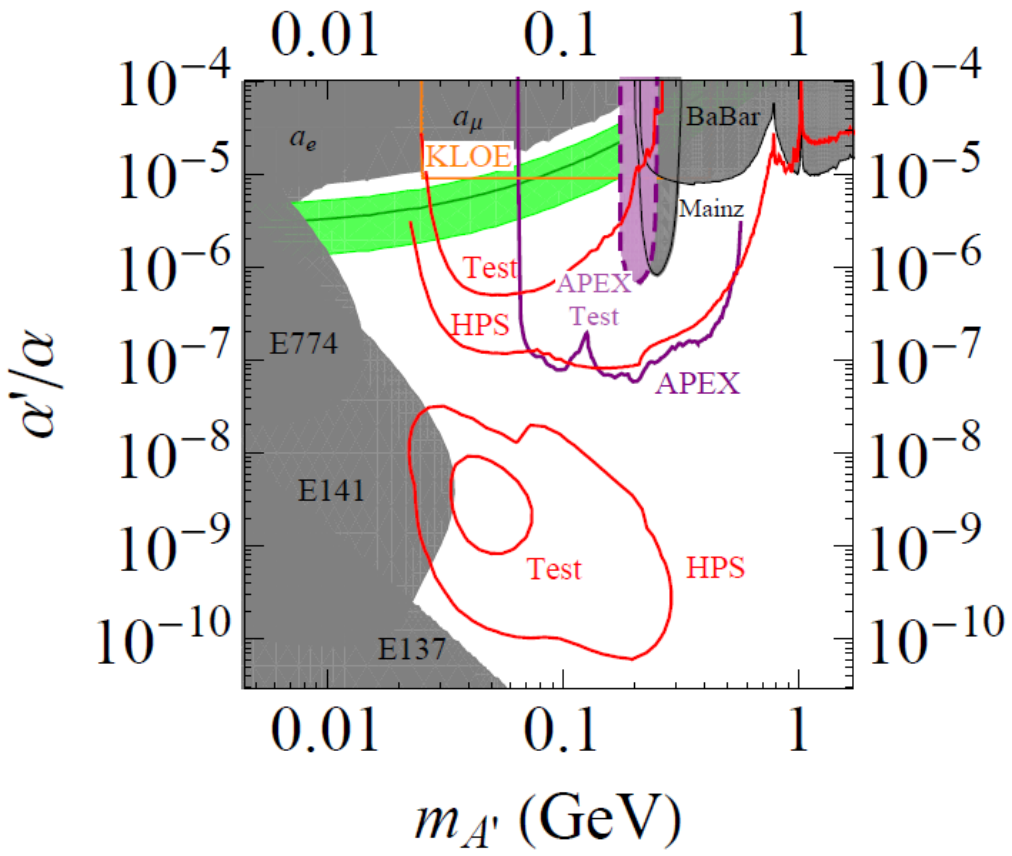

Figure 1.1. Anticipated reach in $\alpha'/\alpha = \varepsilon^2$ for the Heavy Photon Search (HPS) experiment at Hall B in JLab (red lines) with *existing* constraints on an A' from electron and muon anomalous magnetic moment measurements, a_e and a_μ (see [3,4]), the BaBar search for $\Upsilon(3S) \rightarrow \gamma\mu^+\mu^-$ [5], three beam dump experiments, E137, E141, and E774 [6] (see [2]), and a limit from a test run of a fixed target experiment at MAMI (Mainz) [9]. A preliminary limit from a search by KLOE for decays $\Phi \rightarrow \eta\, A' \rightarrow \eta\, e^+\, e^-$ is shown as an orange curve. Note that the limit on a_μ is 5σ, the limit from MAMI is 90%, while the other limits are 95%. The green shaded band shows the ±2σ preferred region for an A' to explain the discrepancy between the observed and Standard Model predicted value for a_μ. Also shown are *estimates* of *potential* 2σ sensitivities for A' searches in existing data (thin dashed lines), assuming optimal sensitivity as described in the full version of this proposal: KTeV $\pi^0 \rightarrow \gamma\, A' \rightarrow \gamma\, e^+\, e^-$, (green dashed curve) and Belle $e^+e^- \rightarrow \gamma\, A' \rightarrow \gamma\, \mu^+\, \mu^-$ (gray dashed curve). In addition, we show the projected 2σ sensitivities for the proposed "APEX" experiment in JLab Hall A (purple) [7], the 2σ projected sensitivity achievable with the APEX test run (purple dashed), and the 5σ sensitivity taken from [8] of the proposed "DarkLight" experiment using the JLab Free-Electron Laser (FEL) (blue). The HPS lines show the combined 2σ sensitivity of two 9×10^6 second runs, with a 6.6 GeV, 450 nA (2.2 GeV, 200 nA) electron beam incident on a 0.25% (or 0.125%) radiation length tungsten target. The Test lines show the 2σ sensitivity of the test run with 0.5×10^6 seconds of beam time. The upper (lower) red curves denote sensitivity of the full resonance search (vertex-based resonance search). The latter lines correspond to 2.4 signal events expected after imposing a vertex requirement that reduces background to 0.5 expected events per resolution-limited mass window. The full detector, trigger, and vertexing efficiencies have been included in these estimates.

Physicists and engineers from SLAC, the Hall B Group at JLab and their collaborators, Fermilab, and UC Santa Cruz have developed both the full HPS proposal, and this HPS Test Run proposal. The full experiment utilizes a high acceptance forward spectrometer with precise momentum, vertexing, and calorimetric measurement capability. Technologically, the HPS depends upon the 40 MHz LHC-style readout capability of the silicon microstrip vertex/tracker, the matching high rate capability of a highly segmented $PbWO_4$ calorimeter, and high rate triggering and data

acquisition systems. Combined with CEBAF's superb duty-cycle, high intensities, and excellent beam properties, this high rate capability lets HPS achieve the high integrated luminosities required to search for heavy photons.

The HPS Test Run will utilize a simplified version of the experiment, but test its crucial aspects. An existing analyzing magnet and vacuum chamber, already in place in Hall B at JLab, will be used in place of the larger magnet proposed for the full experiment. The other chicane magnets are already in place as well. The analyzing magnet will accommodate a simplified tracker-vertexer, which will use only 20 silicon microstrip detectors vs the 120 required for the full design, albeit with reduced acceptance and precision. The electromagnetic calorimeter for the test run will utilize only the existing $PbWO_4$ crystal modules with photodetectors and preamplifiers. The data acquisition system for the tracker/vertexer and the ECal will use the front end components and architecture of the eventual system, but with a much reduced channel count. The data will be taken at 2.2 GeV where the reach extends at most to about 200 MeV/c^2, obviating the need for the muon system, which will be deferred until the full HPS run. The vacuum system is also simplified. An existing vacuum chamber will be modified to accommodate the silicon tracker/vertexer, instead of being built from scratch, and existing beam pipes will be used where possible. The ECal will require construction of a new environmental enclosure and support structure, but they will be reused for the full experiment. The design is discussed in detail below. With all these simplifications, the cost of the test run is approximately one fourth that of the full, unstaged HPS. Many of the costs associated with the test run, including development of the silicon microstrip readout, prototyping the DAQ, and the support and environment control for the ECal, are direct investments in the full HPS.

In the following sections, we first discuss the proposed Test Run experimental setup, including the beamline, silicon tracker/vertexer, ECal, and the electronics and data acquisition systems. Then we review the performance of the apparatus as determined from detailed full Monte Carlo simulations. We conclude with a summary of critical outcomes for the experiment, including its potential reach, and the associated cost, proposed schedules, and personnel that will lead to the timely execution of the HPS Test Run before the scheduled CEBAF downtime.

1.1 References

1. HPS Proposal to JLab PAC37 PR-11-006, http://www.jlab.org/exp_prog/PACpage/PAC37/proposals/Proposals/New%20Proposals/PR-11-006.pdf

2. J.D. Bjorken, R. Essig, P. Schuster, and N. Toro, "New Fixed-Target Experiments to Search for Dark Gauge Forces", Phys. Rev. **D80**, 2009, 075018, arXiv: 0906.0580.

3. M. Pospelov, Secluded U(1) below the weak scale, 0811.1030.

4. Muon G-2 Collaboration, G. W. Bennett et al., Final report of the muon E821 anomalous magnetic moment measurement at BNL, Phys. Rev. D73 (2006) 072003, [hep-ex/0602035].

5. The BABAR Collaboration, B. Aubert, Search for Dimuon Decays of a Light Scalar in Radiative Transitions Y(3S) → γ A0, 0902.2176.

6. J.D. Bjorken et.al., "Search for Neutral Metastable Penetrating Particles Produced in the SLAC Beam Dump", Phys. Rev. D38, 1988, 3375; E.M. Riordan et.al., "A Search for Short Lived Axions in an Electron Beam Dump Experiment", Phys. Rev. Lett., 59, 1987, 755; A. Bross et.al., "A Search for Shortlived Particles Produced in an Electron Beam Dump", Phys. Rev. Lett., 67, 1991, 2942-2945.

7. R. Essig, P. Schuster, N. Toro, B. Wojtsekhowski, "An Electron Fixed Target Experiment to Search for a New Vector Boson A' Decaying to e+e-", arXiv:1001.2557.

8. M. Freytsis, G. Ovanesyan, J. Thaler, "Dark Force Detection in Low Energy e-p Collisions", [arXiv: 0909.2862] JHEP 1001 (2010) 111.

9. H. Merkel et al., Search for light gauge bosons of the dark sector at MAMI", 2011, arXiV: 1101.4091

2 Experimental Setup

2.1 Overview

The HPS Test Run is a simplified, bare bones version of the full HPS apparatus, designed to confirm that backgrounds and trigger rates are as simulated and therefore manageable, but still powerful enough to provide real tracking and vertexing, reasonable acceptance, and full, high rate data acquisition capability. Consequently the HPS Test Run will provide the proof of principle for the full HPS experiment and has the potential to extend the search for heavy photons to as yet unexplored regions of parameter space.

Like the full experiment, the Test Run experiment relies upon the precision measurement of two quantities: the invariant mass of the A′ decay products and the position of the decay vertex. By placing a tracking and vertexing detector immediately downstream of the target inside an analyzing magnet, the complete kinematic information required for A′ reconstruction can be obtained from a single system, whose proximity to the target naturally maximizes the acceptance of a relatively compact detector and provides excellent momentum and vertexing resolution.

The Test Run Tracker replaces the six layer, 120 microstrip sensor design of the full experiment with a five layer system using just 20 sensors over all. Doing so will restrict the acceptance and tracking precision, but retain track finding, momentum measurement, and vertexing capability. Placement of detectors mimics that of the full design. Placing the planes of the tracker immediately downstream of the target means that the intense primary beam must pass directly through the middle of the tracking detector. There are two key consequences of this arrangement. Firstly, scattered beam particles and radiative secondaries are bent by the magnetic field to sweep out a "dead zone" where the particle fluxes would be damaging to the sensors as well as creating an environment too dense for pattern recognition. This necessitates a tracking geometry that keeps the sensors out of this region. However, since the energy released in the decay of a low mass A′ is small relative to its boost, the opening angle between decay daughters can be quite small. Therefore, to maximize the acceptance for low masses, the size of the dead zone must be minimized and sensors placed as close as possible to the beam. Secondly, interactions of the primary beam with air or even helium at atmospheric pressure gives rise to low-momentum secondaries that generate unacceptable occupancies in the detector. The only way to keep the beam in a vacuum without severely compromising acceptance and vertex resolution is to enclose the entire tracking and vertexing system within a vacuum chamber as well. The Test Run apparatus tests both these features.

High luminosities are needed to search for heavy photons with small couplings and masses in the 100 MeV range. Utilizing CEBAF's essentially continuous duty cycle, the experiment can simultaneously maximize luminosity and minimize backgrounds by employing detectors with short livetimes and rapid readout. Silicon tracking sensors are ideal from this perspective, since they collect ionization in 10's of nanoseconds and produce pulses as short as 50-100 nanoseconds. Thanks to electronics developed for the LHC, the sensors can be read out

continuously at 40 MHz. The test run sensors will prototype the designs for the full HPS experiment, utilize the same readout chip, employ the same hybrid, and depend on the same high speed DAQ. The electromagnetic calorimeter just downstream of the tracker uses detectors with comparably short livetimes and high rate capability. It performs two essential functions for the experiment: triggering and electron identification. The device is highly segmented. It is fast, able to readout at rates comparable to those in the tracker, and able to provide good spatial and energy information to the trigger electronics. Like the tracker system, the electromagnetic calorimeter is split to avoid impinging on the "dead zone". The beam and radiative secondaries pass through the calorimeter in vacuum, to avoid generating unnecessary backgrounds. The Test Run Ecal will utilize the existing $PBWO_4$ crystals, existing APDs and readout boards, and DAQ that will be subsequently incorporated into the full experiment. A new temperature-controlled enclosure and ecal vacuum chamber needed for the test run will be re-used for the full HPS run. Only the existing crystals will be used for the test run, so acceptance will be smaller than that for the full HPS, but it will be well-matched to that of the test run tracker and more than adequate for a comprehensive test of trigger rates.

The HPS Test Run will use 2.2 GeV incident electrons and be sensitive to A' masses up to about 150 MeV/c^2. Consequently, the muon system which is part of the full HPS design is not needed for the Test Run, and its construction will be deferred until higher energies are run. This system is perhaps the most conventional and robust of the detector systems in HPS, and the one least stressed by extreme background or rate conditions. So its omission in the Test Run does not compromise our checks of future HPS capability in any significant way.

The various elements of the experiment are discussed in more detail below, beginning with the beamline, continuing with the tracker/vertexer, electromagnetic calorimeter, and concluding with the electronics and DAQ.

2.2 Beamline Elements

2.2.1 Layout

The HPS test experiment will utilize a setup located upstream of the CLAS detector. It will use the same three magnet chicane that is used for the CLAS two photon exchange experiment (TPE). The layout of the beam line and the chicane is shown in Figure 2.2.1.1. The Hall B pair spectrometer magnet, 18D36 (pole length 91.44 cm, max-field 1.5 T), will serve as the analyzing magnet. The dipole field direction (Y) is perpendicular to the horizontal (XZ) plane. A Hall B "Frascati" H magnets (pole length 50 cm, max-field 1.2 T) will be used as the first and the last dipoles of the chicane. The analyzing magnet will be operated at a 0.5T-m field. The two bending magnets will be set to 0.25T-m fields. The distance between the centers of the magnets and the location of the chicane will be exactly the same as for the TPE run. The only change that will be made to the TPE chicane layout is a transverse displacement of the analyzing magnet by about 4 inches (to beam left) in order to optimize the detector acceptance for e^+ and e^-.

The detector package will include five layers of silicon detectors, mounted inside the vacuum box in the high field region of the analyzing magnet, see Figure 2.2.1.2. The existing vacuum box of the Hall B pair spectrometer will be used to host the tracker and the target. The silicon tracker is described in Section 2.3 below. Downstream of the analyzing magnet there will be an electromagnetic calorimeter for triggering, and for electron and positron identification (see Section 2.4). The target foil will be positioned at the beginning of the analyzing dipole pole. The distance from the target to the first layer of the silicon tracker will be 10 cm. The distance from the target to the face of the electromagnetic calorimeter is ~137 cm. There will be continuous vacuum for the electron beam line through the entire setup ending in the Hall B electron beam dump.

Since the chicane layout is the same as for the TPE run, no new equipment is needed to run the chicane. The analyzing magnet, the Hall B pair spectrometer dipole, has its own power supply. The "Frascati" H magnets will use one common power supply that will be borrowed from the Hall B Moller polarimeter. There will be a shunt installed between the two "Frascati" magnets to allow independent small changes in currents on those two magnets (as it was done during the TPE experiment). Both power supplies are bipolar, so the magnets can be degaussed when needed.

New beam line elements that will be needed for the HPS test run are the upstream flange of the vacuum box of the analyzing magnet, a vacuum chamber between the top and bottom parts of the calorimeter that will be connected to the tracker vacuum box, and a vacuum box behind the calorimeter through the third magnet. For the beam line upstream of the analyzing magnet vacuum box and downstream of the third magnet, the standard vacuum beam line of Hall B, with a few small modifications, will be used.

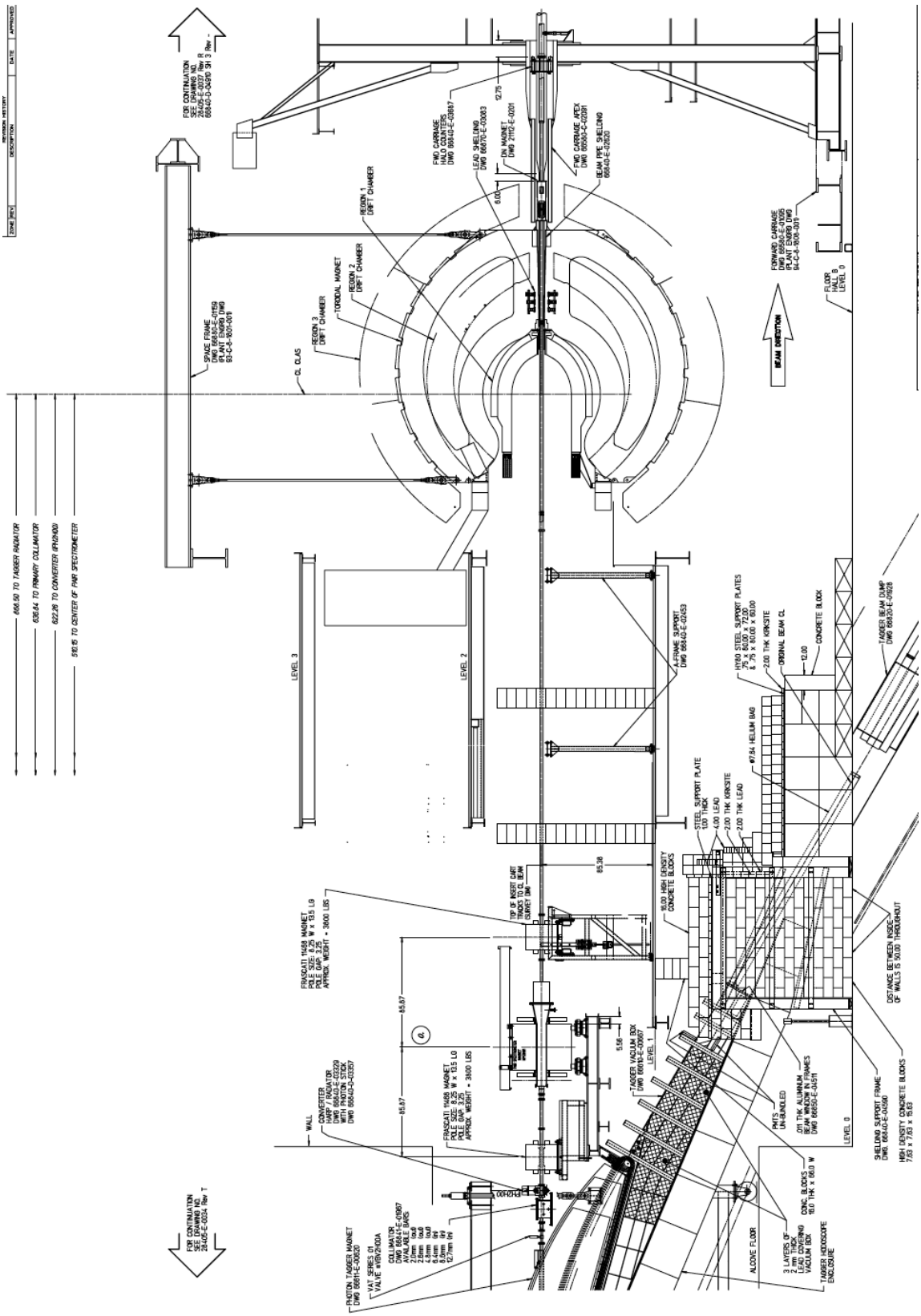

Figure 2.2.1.1. Layout of the HPS test run setup upstream the CLAS detector

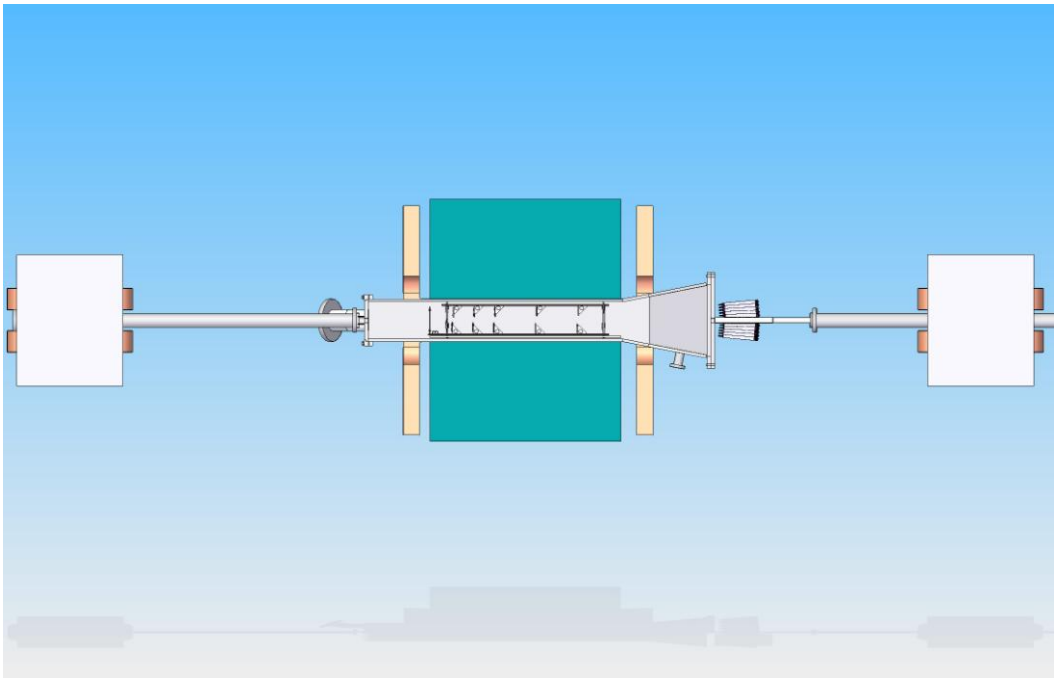

Figure 2.2.1.2. Layout of the HPS test run chicane and detector package.

2.2.2 **Running Conditions**

HPS test run will use ~2.2 GeV electron beam incident on a tungsten (W) target. Beam currents of up to 200nA will be used on tungsten target foils with thicknesses from 4μm (0.125% RL) to 8μm (0.25% RL). The high intensity electron beam incident on the tungsten target will generate a significant amount of electromagnetic radiation, composed mainly of bremsstrahlung photons, electrons which have radiated, Moller electrons, and beam particles which have multiple Coulomb scattered. In the dipole field, this radiation will create a "sheet of flame" in the bending plane (XZ), at the beam height, Y≈0. Detectors will be positioned above and below the beam plane, leaving a small gap for the bremsstrahlung and multiple Coulomb scattered beam and beam backgrounds to pass through. The gap between the upper and lower planes of the silicon tracker will be approximately ±15 mrad. This angular gap will be maintained between the upper and lower parts of the calorimeter as well.

Operational experience shows that the CEBAF beam is very clean, and is contained within ±1mm with halo at the level of less than 10^{-5}, so it will easily pass through the "dead zone" gap. In Figure 2.2.2.1 the beam profile measured using a wire harp during one of the recent CLAS experiments at 2.2 GeV is presented. Beam sizes of < 100 μm are typical for the B-line. It should be noted that the profile measured with the wire scanner includes not only the actual beam size but also any >100 Hz beam motion. Studies are needed to decouple beam motion from the actual beam size

The beam sizes presently achievable in Hall B are suitable for much of the test run. However, for checking the vertexing performance and acquiring physics data, an asymmetric beam profile is

desirable. Since the vertex resolution in the non-bend plane will be high, beam sizes of 20-30 μm in the Y direction are preferable. The momentum measurement will not benefit from small beam sizes in the X direction, and small beam sizes in both dimensions will overheat the target foil. For these reasons the required beam sizes for part of the run will be σ_X ~ 250 μm and σ_Y ~ 30 μm.

The HPS beam parameter requirements are presented in Table 2.2.2.1.

Parameter	Requirement/Expectation	Unit
E	2200	MeV
$\delta p/p$	$< 10^{-4}$	
Current	< 200	nA
Current Instability	< 5	%
σ_x	< 300	μm
σ_y	< 40	μm
Position Stability	< 30	μm
Divergence	< 100	μrad
Beam Halo (> 5σ)	$< 10^{-5}$	

Table 2.2.2.1 Required beam parameters.

None of the CLAS experiments have requested such small (20-30 μm) beam sizes. The optics program ELEGANT is used to determine the optimized element parameters of the B-line optics in order to achieve these beam sizes at the HPS test run target location. An emittance of $\varepsilon_x = 1x10^{-9}$ m-rad and $\varepsilon_y = 1x10^{-9}$ m-rad are used as input. These values are a factor of three larger than the design values so the beam size could be smaller by √3 if the emittance is near the design value. The results from the first optimization run for the horizontal and vertical beam sizes for a 2 pass beam at 2.2 GeV are shown in Figure 2.2.3.2. The goal of the optimization was to achieve the smallest possible beam sizes in both X and Y. With the existing B-line optics, beam sizes of ~30 μm is achievable. The second optimization run determined beamline parameters for an asymmetric beam. Results of this optimization are presented in Figure 2.2.3.3. An asymmetric beam profile with σ_X ≈250 μm and σ_Y≈20 μm is also achievable.

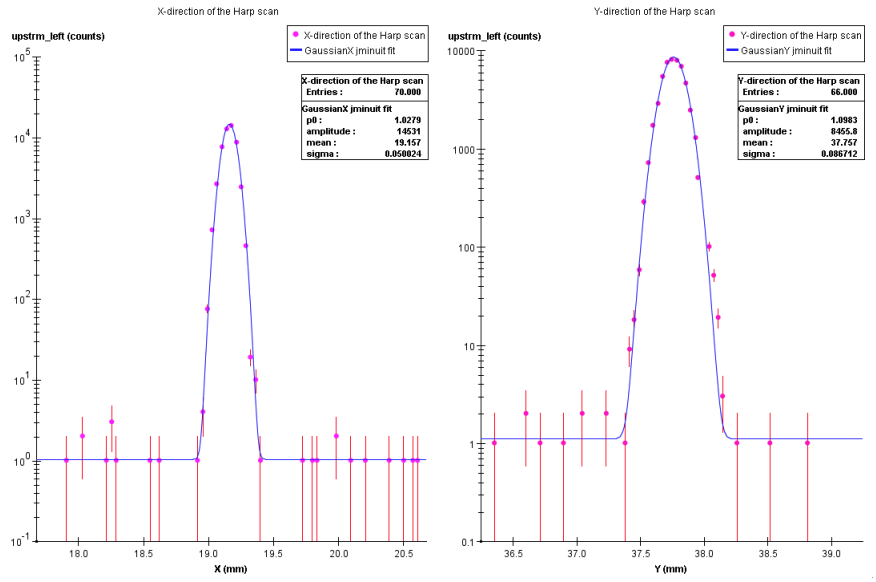

Figure 2.2.2.1: Hall B 2.2GeV beam profile measured during one of recent CLAS experiment.

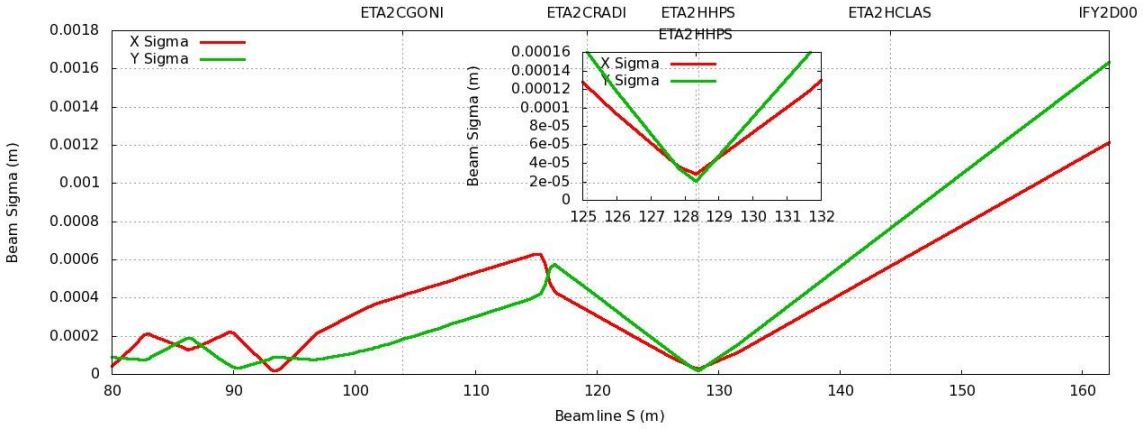

Figure 2.2.3.2. Beam sizes in X and Y along the B-line in the upstream tunnel and in the region of the HPS test run setup. At the HPS target beam size of σ~30μm can be achieved with existing B-line optics.

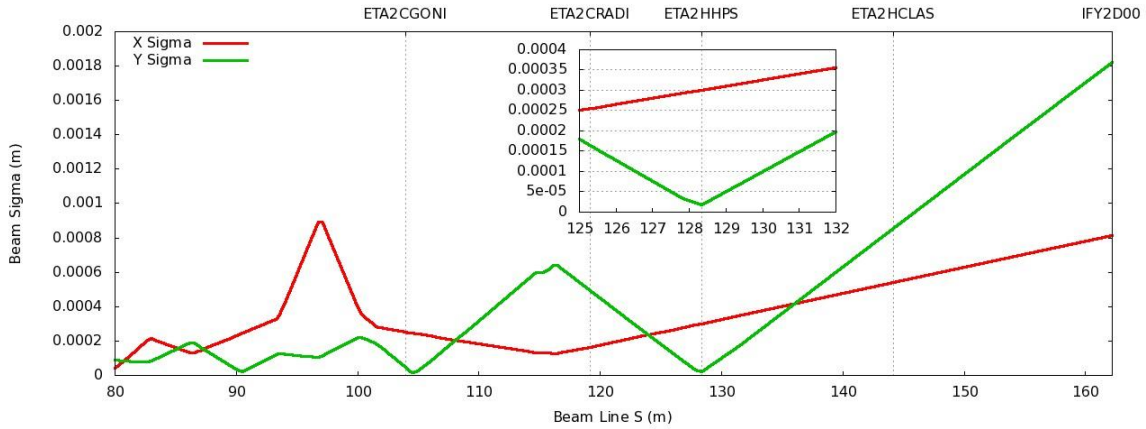

Figure 2.2.3.3. Beam sizes in X and Y along the B-line in the upstream tunnel and in the region of the HPS test run setup. At the HPS target asymmetric beam profile σ_X=300μm and σ_Y=20μm can be achieved with existing B-line optics.

2.2.3 **Diagnostics and Trajectory Control**

The HPS test run will use the Hall-B beam line as is. Beam position and current will be controlled by two sets of cavity beam position monitors (BPM) that are located in upstream tunnel. There are sets of corrector dipoles and quadrupoles that are routinely used to tune the beam for Hall B. Pair of BPMs will define the incoming trajectory of the beam and are in the fast feedback loop. Readings from these BPMs will be used to maintain stable beam position and current.

The beam profile will be measured using two wire scanners, one installed in front of the first chicane dipole, another about 8 meters upstream. These two profilers will be used to establish the required beam parameters. There will also be a wire scanner mounted on the target ladder to check the beam profile at the target location.

There will be set of beam halo counters mounted along the beam line in order to provide fast monitoring of the beam conditions. These counters are like those used for beam profile measurements. They are also included in the machine fast shutdown system (FSD) in order to terminate beam in the event of beam excursions.

2.2.4 **Targets**

Thin tungsten foil will be used for the target. High Z material is chosen to minimize the hadronic production relative to the trident and A′ production, since the ratio of QED to hadronic processes goes as (Z^2/A). The target will be located 10 cm in front of the first plane of silicon strip detectors. The primary target will be 0.125% of a radiation length (approximately 4 microns tungsten). A foil of 0.25% radiation length will also be available for some of the data taking, adjusting the beam current as appropriate.

It is intended to operate with beam currents up to 200 nA, which will produce strong local heating in the target. The strength of tungsten drops by an order of magnitude with temperature increases in the range of 1000° C. In addition, the material re-crystallizes above this range, which increases the tendency for cracking where thermal expansion has caused temporary dimpling. For these reasons, we plan to keep the temperature rise below about 1000 degrees. This can be accomplished by keeping the beam Gaussian width above 70 microns for a round beam spot. However, a strongly elliptical beam spot will be an advantage for constraining the vertex during data analysis. A spot of, for example, 20 by 250 microns would achieve the same limitation of the temperature rise.

The combination of vacuum, magnetic field and potential radiation damage have to be borne in mind in the design, and suitable materials must be used. The device additionally has to be compatible with the silicon strip detector system and its cable and cooling plant, as well as beam line diagnostic equipment.

A vertical linear motion mechanism will allow the foil to be positioned on or off the beam line. The foil material will be mounted on a 3-sided frame, the upper edge being free-standing. That will be the leading edge when the foil is moved up on to the beam line, and so the move can be made without inhibiting the beam delivery, which would be necessary if a full rectangle were to be used for the frame. Alignment relative to the beam is thus easily accomplished. Between the supports, the surface of the foil will be 5 mm tall by 20 mm wide.

By providing position control, further advantages can be realized. Lower on the same C-frame, separated by 1 millimeter, will be a second foil of probably 8 microns (0.25% radiation length) to further test scaling of the detector performance against thickness and beam current. However, in addition, a set of tungsten wires will be installed on extensions of the arms of the support frame. The wires, of about 12 microns diameter, will in fact be the first material to encounter the beam during insertion. They will be used as a fairly conventional wire scanner. In particular they would be able to provide information about the minor and major axes, and the tip angle (roll), of a strongly elliptical beam spot. Wires mounted at ±6° and horizontal would be ideal for this purpose. They will be spaced to avoid overlap between scan profiles for the largest beams they are required to measure. There is adequate room for this. Positioning resolution of 5-10 microns will be provided for scanning. It is intended to read out scatter signals from the wires by using some of the calorimeter crystals. If these signals are not within range, a simple counter will be installed for the purpose at the downstream end of the vacuum tank.

2.2.5 **The scattering chamber**

One of the critical elements on the beam line is a scattering chamber between the top and bottom parts of the ECal. In order to keep calorimeter coverage close to the beam, maintain required thickness of the thermal insulation for ECal, and maintain as wide as possible vacuum gap, the

top and bottom plates of the scattering chamber must be quite thin. At the locations of primary beams (e^- and γ) the openings in the chamber must be even bigger.

In Figure 2.2.5.1 a conceptual design of the scattering chamber is shown. Front flange of the chamber matches to the exit flange of the vacuum box inside the analyzing magnet. Vacuum is maintained only on the electron side (beam right). Two wider openings are for electron and photon beams. This design allows crystals to be at 20 mm from the beam plane. After the crystals, some where at half a length of the chamber, vacuum chamber plates will be thicker since there is no need for electronics to be at the same level as the crystals.

Figure 2.2.5.2 shows this arrangement with the crystals at 20 mm of the beam, and in between the thermal shield of the ECal surrounding the chamber wall and reinforcement rib closed to the elliptical shape.

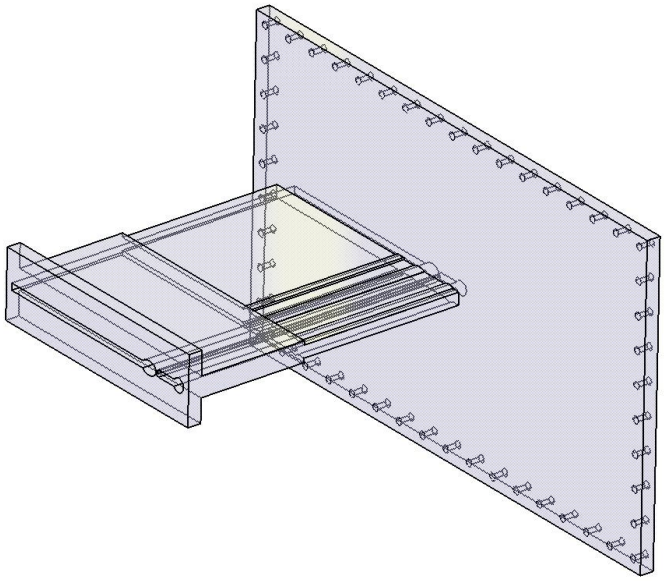

Figure 2.2.5.1. A conceptual design of the scattering chamber.

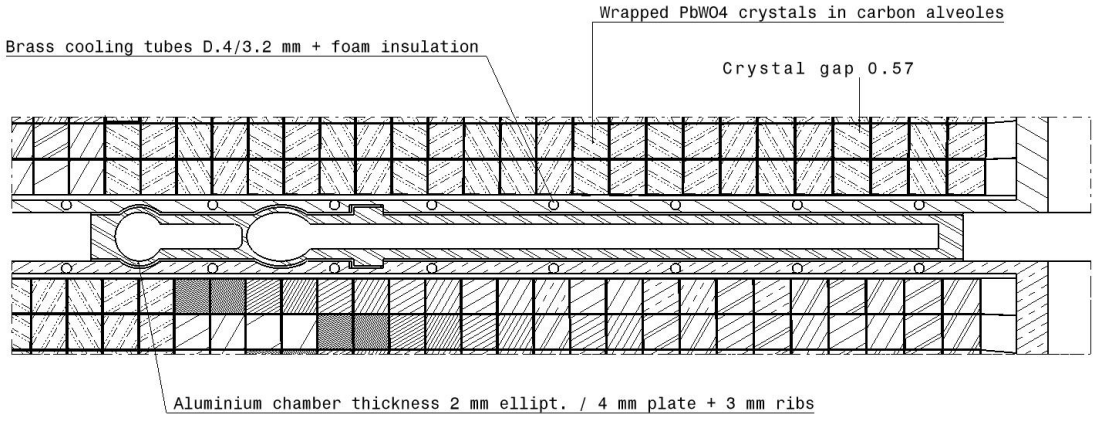

Figure 2.2.5.2. Special arrangement to fit the scattering chamber with the ECAL.

In order to validate the conceptual design physics simulations and mechanical analysis are performed. The proposed chamber can be made of aluminum 5083 H111 or stainless steel 304 L. In Figure 2.2.5.3 stress analysis performed with an aluminum chamber, which follows the CODAP design rules is shown. In Figure 2.2.5.4, the deformation in the middle is shown. One of possible solution to avoid the deformation can be inserting an aluminum honeycomb in the scattering chamber. Further physics simulations and mechanical optimization are foreseen.

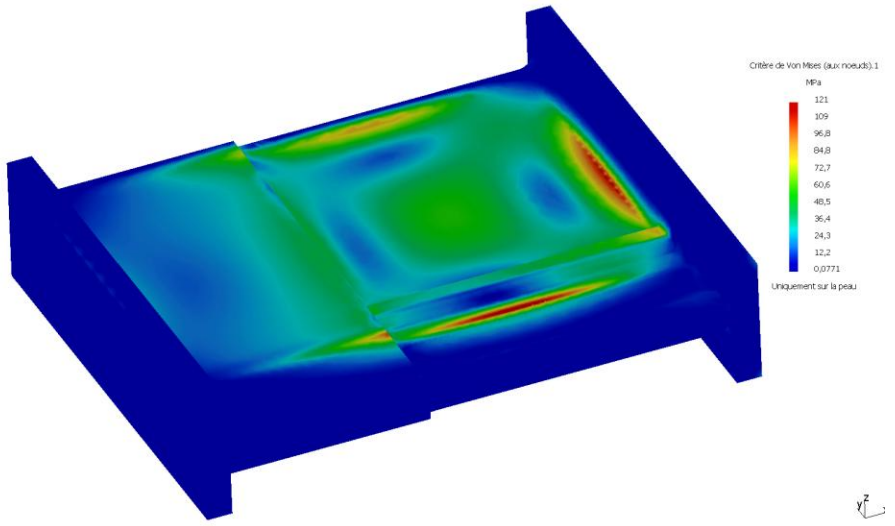

Figure 2.2.5.3. The stress analysis of the proposed scattering chamber made of aluminum 5083.

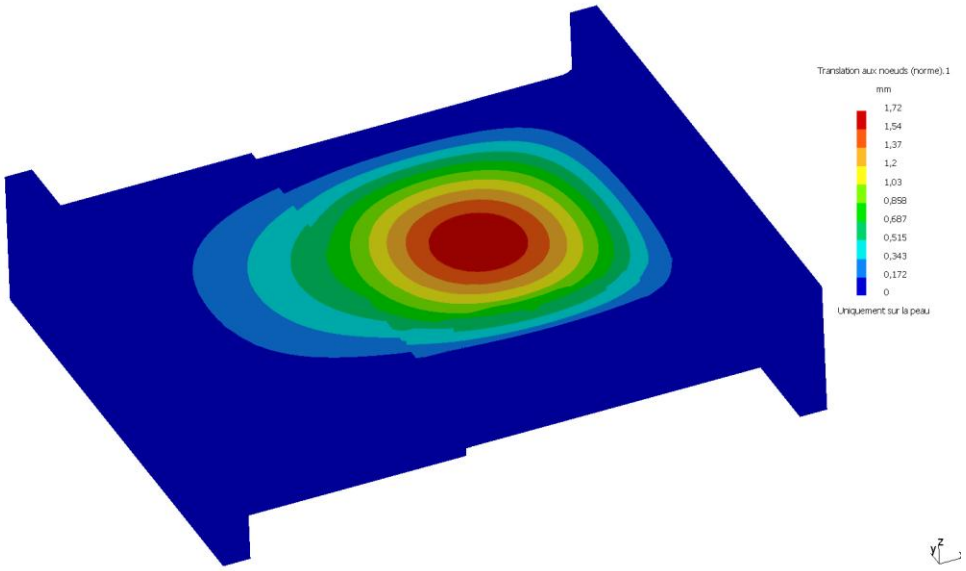

Figure 2.2.5.4. Deformation of the top and bottom plates of the vacuum chamber.

2.3 Tracking and Vertexing System

2.3.1 Design Considerations

A critical objective of the test run is establishing that the tracker can be built as conceived and that the backgrounds it encounters are acceptable for the full experiment. The more ambitious goal of achieving sensitivity to a hidden sector photon with data from the test run naturally promotes these objectives and presents considerable challenges. At the beam energies necessary to achieve sensitivity to A′ in the interesting mass range, the decay products will be electrons with momenta on the order of a few GeV/c. Consequently, multiple scattering dominates the key measurement uncertainties for any feasible material budget and, for both the mass and vertexing resolutions, the radiation lengths of material must be minimized throughout the tracker. To minimize the impact of beam backgrounds, the tracker is split into upper and lower half-planes which avoid the "dead zone" defined by the beam envelope and those electrons which have radiated in the target. To avoid secondary backgrounds which would arise from the passage of the beam through gas, the beam must be transported in vacuum and the entire tracker placed within a vacuum chamber. Finally, the position and tails of the beam profile may not be exactly known and there are significant uncertainties in the background estimates and the radiation tolerance of the sensors for the background environment. So, it will be important to be able to adjust the position of the tracking planes remotely. It is also sensible to provide for access to the tracker with minimal intervention, to accommodate repairs or replacement of tracking planes.

2.3.2 Sensors

The high rate and intense radiation in the tracking volume, together with the requirement for precision vertexing necessitate the use of silicon sensors for the tracker. The key requirements are low mass, high radiation tolerance, fine readout granularity and the ability to instrument large areas at a reasonable cost. The convergence of these requirements leads to the use of silicon microstrip detectors.

A large supply of suitable sensors is available, remaining from the cancelled Run IIb upgrades of the DØ and CDF detectors at the Tevatron [1]. These are p+ on n, single sided, AC coupled, polysilicon-biased sensors fabricated on <100> silicon. The relevant specifications of these sensors is shown in Table 2.3.2.1. While the specifications only ensure that these sensors may be operated up to 350V bias after irradiation, previous experience indicates that many of them will be operable to 1000V and therefore remain fully depleted to a dose of approximately 1.5×10^{14} 1MeV neq/cm^2. Although this level of radiation tolerance is not required for the test run, we intend to verify our ability to operate the sensors at high bias voltages before the end of the run.

Cut Dimensions (L×W)	100 mm × 40.34mm
Active Area (L×W)	98.33 mm × 38.34mm
Readout (Sense) Pitch	60μm (30μm)
# Readout (Sense) Strips	639 (1277)
Depletion Voltage	40V < V_{dep} < 300V
Breakdown Voltage	>350V
Total Detector Current at 350V bias	<16 μA
Bias Resistor Value (both ends of strips)	0.8 ± 0.3 MΩ
AC Coupling Capacitance	>12 pF/cm
Total Interstrip Capacitance	<1.2 pF/cm
Defective Channels	<1%

Table 2.3.2.1: Specifications of sensors available for this experiment. Many of the sensors exceed the bias voltage and bad channel specifications by a significant margin.

2.3.3 **Readout Electronics**

The extreme occupancies in the tracker demand the shortest possible readout integration time with the best possible time resolution. Since the development of a front-end readout chip is well beyond the scope of even the full experiment, existing front-end chips designed for the LHC tracking detectors are the obvious choices. Of these, the APV25, originally developed for use by the CMS tracker, is the most attractive option [2]. The relevant specifications of the chip are summarized in Table 2.3.3.1.

# Readout Channels	128
Input Pitch	44 μm
Shaping Time	50ns nominal (35ns min.)
Output Format	multiplexed analog
Noise Performance (multi-peak mode)	270+36×C(pF) e- ENC
Power Consumption	345 mW
Communication Protocol	I^2C

Table 2.3.3.1: Specifications of APV25 Readout ASIC.

The first desirable attribute is excellent noise performance, largely due to the inherent properties of the 0.25μm fabrication process. High signal-to-noise ratio in the detector results in high single-hit efficiency with a low rate of noise hits and extremely good single-hit spatial resolution. Before irradiation, the signal-to-noise ratio with the sensors will be approximately 34, resulting in full single hit efficiency with a negligible rate of noise hits. Single-hit resolution will be approximately 6 μm based upon test beam and simulation with similar sensors [3].

The second desirable attribute naturally arising from the 0.25 micron fabrication process is a high degree of radiation tolerance. Although the readout chips are expected to see much

smaller doses than the hottest regions on the sensors, some chips will see doses that would result in performance degradation of chips that are not radiation tolerant.

Finally, and most importantly here, the APV25 has a flexible readout architecture, which can be used to improve the time resolution of hits in the tracker. In addition to the standard readout modes employed at the LHC, the APV25 may be operated in "multi-peak" mode, in which the output of the shaper (with nominal shaping time of 50ns) is sampled at clock-synchronous 25ns intervals, in multiples of three samples, after a trigger is received [4]. Fitting the known form of the shaper output curve to these samples allows the determination of both the peak amplitude and the t_0 of the hit. Tests have shown that at S/N>25, the hit time may be reconstructed with an RMS of 2ns or better for the readout of three samples [5].

The APV25 chips will be hosted in groups of five on hybrid circuit boards, often simply referred to as "hybrids." In order to reduce the amount of effort in developing them, we are using existing APV25 hybrid designs as a starting point. Since the readout electronics for this experiment will not reside within the tracking volume, the material budget for the hybrids and the cooling they require is less constrained. It is therefore anticipated that the hybrids will be fabricated in standard FR4 or polyamide rather than exotic ceramics, which broadens vendor selection, reduces cost and saves turnaround time. In addition to reducing schedule risk, this will allow a prototype run to ensure that the hybrid design is sufficient without incurring significant additional costs.

2.3.4 **Detector Layout**

There are five measurement stations, or "layers", placed immediately downstream of the target. Each layer is comprised of a pair of closely-spaced planes and each plane is responsible for measuring a single coordinate, or "view". The details of the five layers are shown in Table 2.3.4.1 and a conceptual rendering is shown in Figure 2.3.4.1. Altogether, this layout comprises 20 sensors and hybrids and 100 APV25 chips for a total of 12780 readout channels. The existing vacuum chamber to be used for the test run cannot accommodate the 90-degree stereo layers used in the full experiment to optimize the vertex resolution. Instead, 100 milliradian stereo is used in the first three layers to provide higher-resolution 3-d space points for vertexing. The 50 milliradian stereo of the last two layers minimizes fakes from ghost hits, improving pattern recognition while still providing sufficient pointing resolution into Layer 3 for robust hit association in the denser environment there. As discussed in Section 3.3 the pattern recognition of this layout is robust and the vertexing and momentum resolution are sufficient to provide the necessary sensitivity.

	Layer 1	Layer 2	Layer 3	Layer 4	Layer 5
z position, from target (cm)	10	20	30	50	70
Stereo Angle	100 mrad	100 mrad	100 mrad	50 mrad	50 mrad

Non-Bend Resolution (μm)	≈ 6	≈ 6	≈ 6	≈ 6	≈ 6
Bend-Plane Resolution (μm)	≈ 60	≈ 60	≈ 60	≈ 120	≈ 120
# Sensors	4	4	4	4	4
Dead Zone (mm)	±1.5	±3.0	±4.5	±7.5	±10.5
Power Consumption (W)	6.9	6.9	6.9	6.9	6.9

Table 2.3.4.1: Key parameters of the sensor layout for the tracking and vertexing system. Notice that the excellent single-hit resolution in the measured view enables good stereo resolution at the relatively small stereo angles necessary to fit in the existing vacuum chamber. The stay clear region for the primary beam creates a "dead zone" in the tracker on either side of y=0.

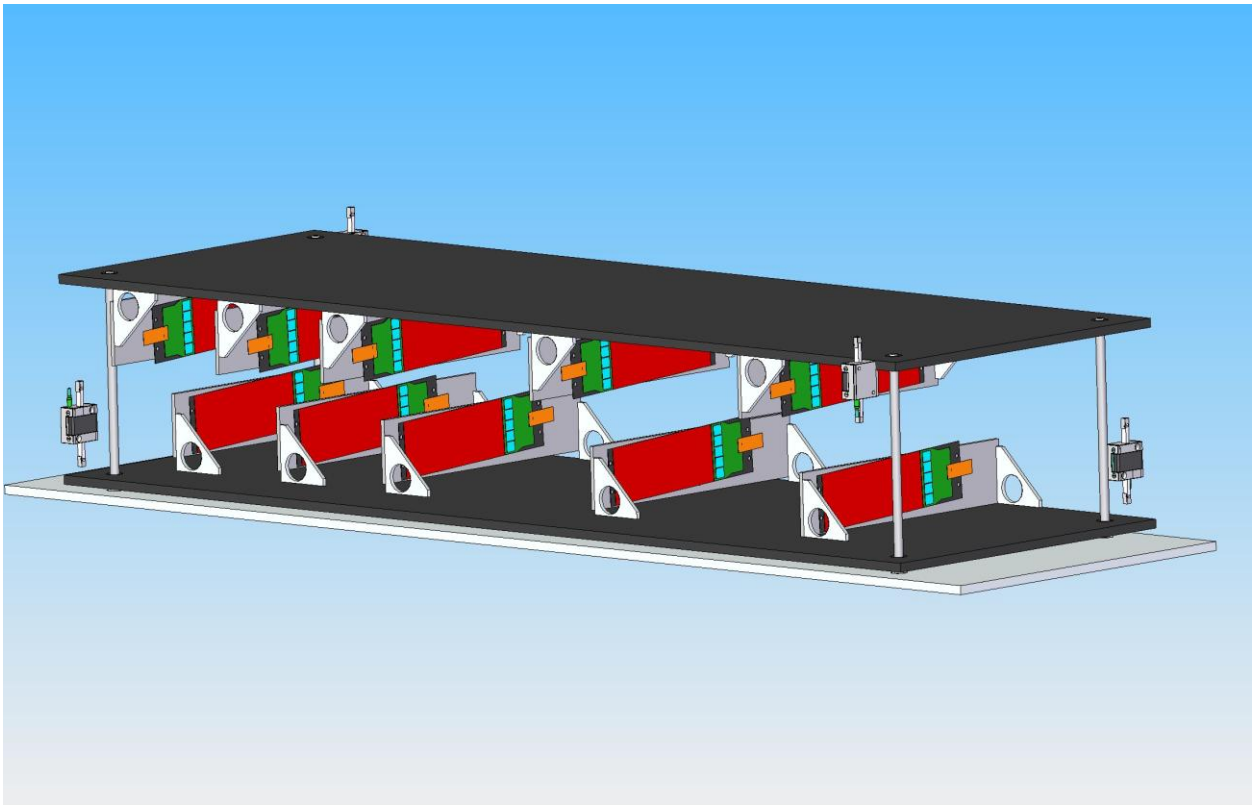

Figure 2.3.4.1: A rendering of the tracker showing the layout of the silicon planes mounted to the upper and lower support plates. The elevation and slope of each plate is adjusted by a pair of motors to adapt the dead zone to beam conditions. The target assembly is 10 cm upstream of the first silicon layer.

As shown by Figure 2.3.4.2, the solid angle subtended by the dead zone limits the acceptance for low mass A′ decays, which have very small opening angles between decay daughters. For this reason, a great deal of attention has been paid to the optimization of this region of the detector, where careful simulation of the backgrounds has been used to determine the occupancies and radiation doses that limit coverage there. However, uncertainties in these simulations are a major source of uncertainty in the acceptance that can be achieved, with GEANT4 and EGS5 disagreeing by roughly a factor of two as shown in Figure 2.3.4.3.

Measuring the distribution of scattered beam that defines the dead zone is therefore a key goal of operating the tracker in the test run.

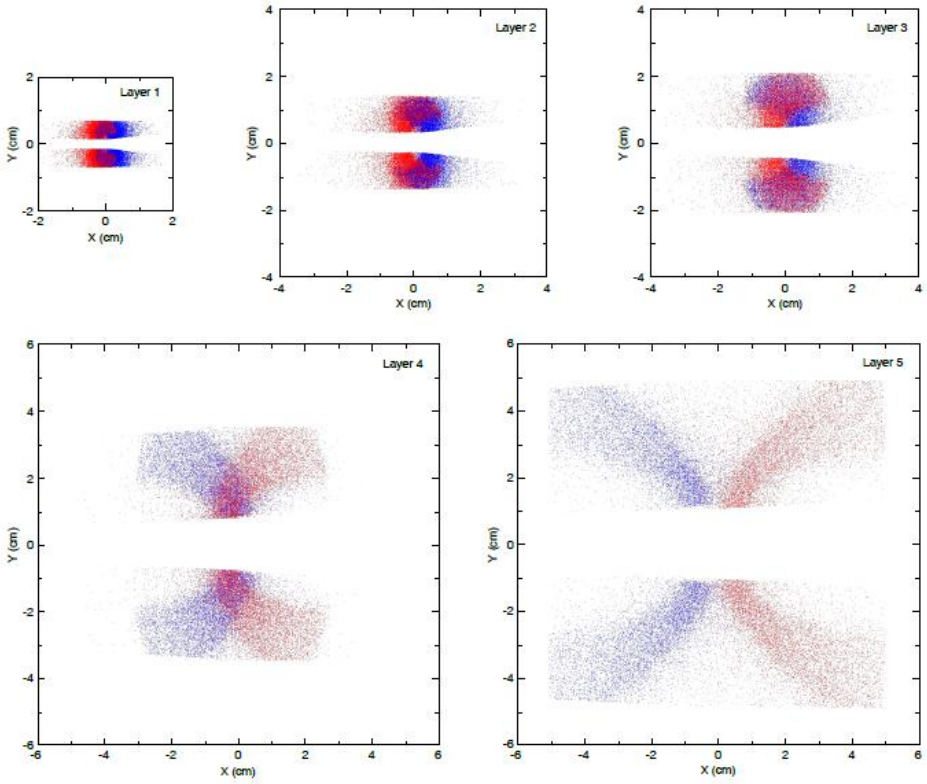

Figure 2.3.4.2: Hits in the silicon tracker in all five layers produced by A′ decays with $m_{A'}$ = 100 MeV/c^2 and E_{beam} = 2.2 GeV. Tracks that hit all five layers are shown, resulting in a five-layer A′ acceptance of 12% in the 0.5T magnetic field. Most of the tracks within the tracker acceptance are also accepted by the calorimeter.

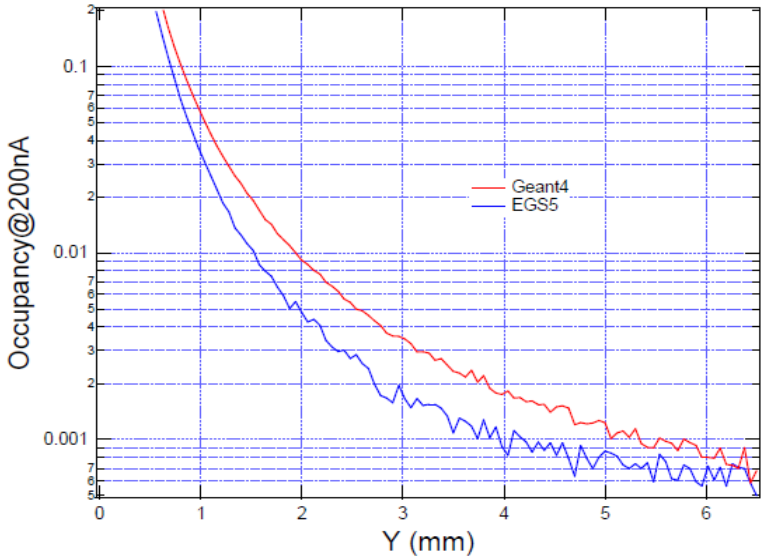

Figure 2.3.4.3: The hit occupancy per strip for 60 μm strips in Layer 1 for 7.5 ns of beam at 200nA intensity as predicted by GEANT4 and EGS5.

For the full experiment, a dead zone of +/-1.5 mm in Layer 1, corresponding to 15 mrad for prompt decays, is close to optimal from all perspectives. While the lower radiation dose of the

test run might allow for a slightly smaller dead zone, little acceptance can be gained without risking passage of the primary, unscattered beam through the guard region of the silicon: even with a ± 1.5 mm dead zone in Layer 1, the cut edge of the silicon sensors lie only 500 microns from the center of the beam. Since we can verify our assumptions about the background environment and occupancies for the full run with a 15 mrad dead zone, this is the default plan for the test run. However, with large uncertainties in the actual occupancies, the capability to adjust the dead zone as needed will be of significant value for the physics, as well as for the safety of the detector during beam setup.

2.3.5 **Sensor Modules and Mechanical Support**

Each of the ten planes that measures a single view is split into two modules, upper and lower, to accommodate the horizontal dead zone that cuts the entire tracker in half. These modules are the fundamental mechanical units of the detector: the components of a module are permanently bonded together during assembly. Each consists of a pair of silicon sensors and their hybrid circuit boards glued to a composite support structure.

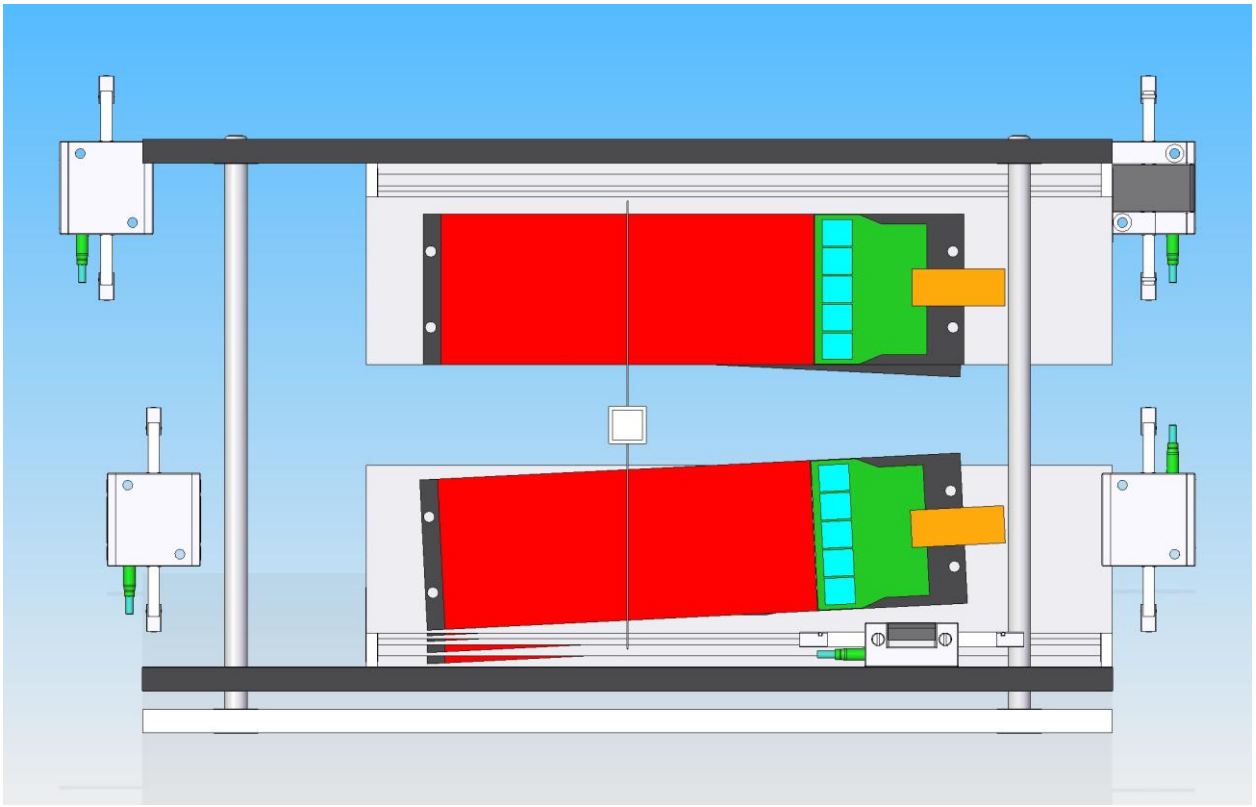

Figure 2.3.5.1: A rendering of the view looking upstream at Layer 5 in the tracker. The sensors (red), hybrids (green), APV25 chips (blue) and hybrid pigtails (gold) are all shown along with the carbon fiber support backings (black) and rohacell (gray) that together comprise the modules. The motors and rails that allow vertical motion of the support plates holding the tracker modules are also shown.

The sensors comprising a stereo pair are placed on opposite sides of the structure with the stereo angle above and below the dead zone signed to maximize the distance between the stereo sensors and the low-energy tail of the scattered beam as illustrated by Figure 2.3.5.1. At the end of each sensor is the hybrid circuit board containing the five APV25 readout ASICs

necessary to read out the signals from a single sensor. The pitch of the APV25 and the sensors are similar enough that a pitch adapter can be avoided here: wire bonds can be made directly from the chips to the sensors.

Each module support structure is comprised of a pair of thin, high-modulus, carbon fiber composite skins sandwiched around a low-mass rohacell core. At the edges of the support structures, running underneath the readout chips, are integrated stainless-steel cooling tubes carrying water-glycol coolant at approximately -5°C to remove the 1.7W heat load generated by each hybrid. The cooling tubes are in contact with the skins on both module faces to cool the silicon. The unidirectional carbon fiber of the skins are oriented to efficiently transport heat from the silicon to the cooling tubes. This arrangement provides sufficient cooling for the silicon without placing cooling tubes inside the tracking volume that would increase multiple coulomb scattering and compromise sensitivity.

Atop the carbon fiber, there is a layer of pyrolytic graphite sheet that improves thermal conductivity and includes a layer of PEEK passivation rated at 2kV to isolate the back side of the sensors, which are at high voltage, from the conductive graphite [11]. The layers of carbon fiber and graphite will have a low-impedance connection to the analog ground of the readout electronics to ensure the best possible noise performance.

The individual planes on each side of the dead zone are mounted on a pair of base plates via small angle brackets, as shown in Figure 2.3.5.2. These brackets allow for manual positioning and alignment of the tracker planes relative to one another during assembly so that the active edges of the silicon in all layers define a plane at the boundary of the dead zone. The cables and cooling lines that attach to the pigtail cables and cooling connections of each sensor module will be semi-permanently installed on the base plates. This minimizes the difficulty of installing and removing sensor modules and simplifies insertion and extraction of the tracker to and from the vacuum chamber.

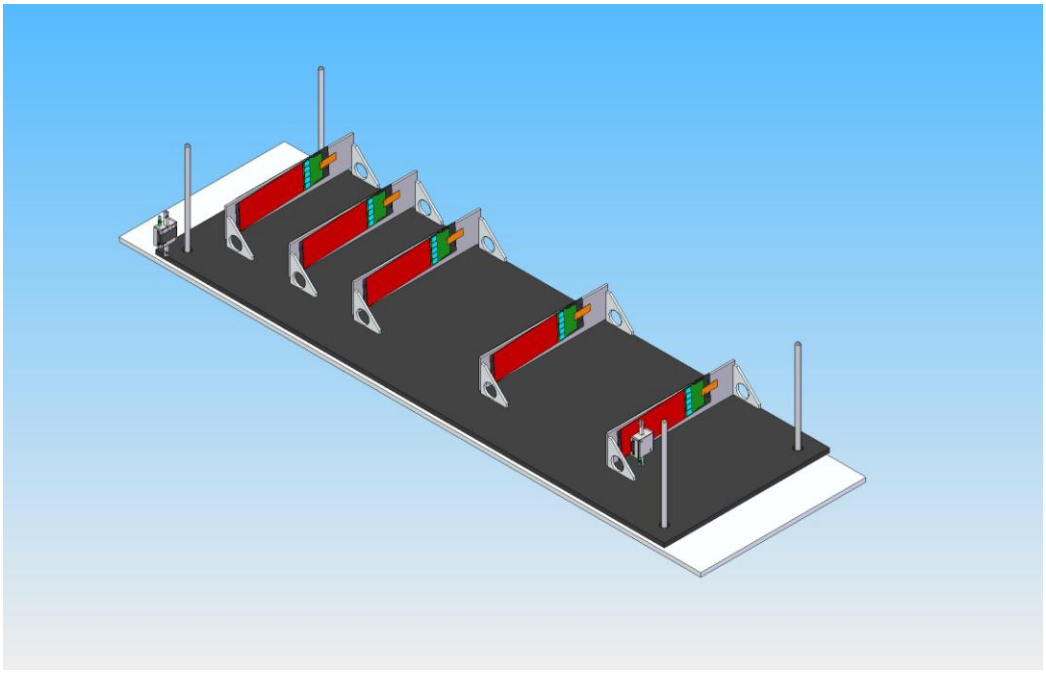

Figure 2.3.5.2: A rendering of the tracker showing the support plate and module mounting brackets.

Each base plate will be movable via a pair of remotely-controlled vertical stages at the front and back ends of the tracking volume. These allow the tracker to be opened up during beam setup and allow tuning of the dead zone in response to background conditions.

2.3.6 **Vacuum Chamber**

The tracker for the test run is designed to fit within the existing vacuum chamber for the Hall B TPE chicane as described in Section 2.2. A new flange will be fabricated for the front of the vacuum chamber to accommodate a connection to the beampipe as well as a pair of smaller flanges on either side of the entering beam with patch panels for cables and cooling as shown in Figure 2.3.6.1. These flanges can accommodate a total of eight 50-pin, vacuum rated, D-connectors to carry power, control and data signals, and high voltage to and from the detector as well as cooling for the detector and power for the positioning stages. Removal of a short section of upstream beampipe and the front flange allows for easy insertion and extraction of the target and the tracker.

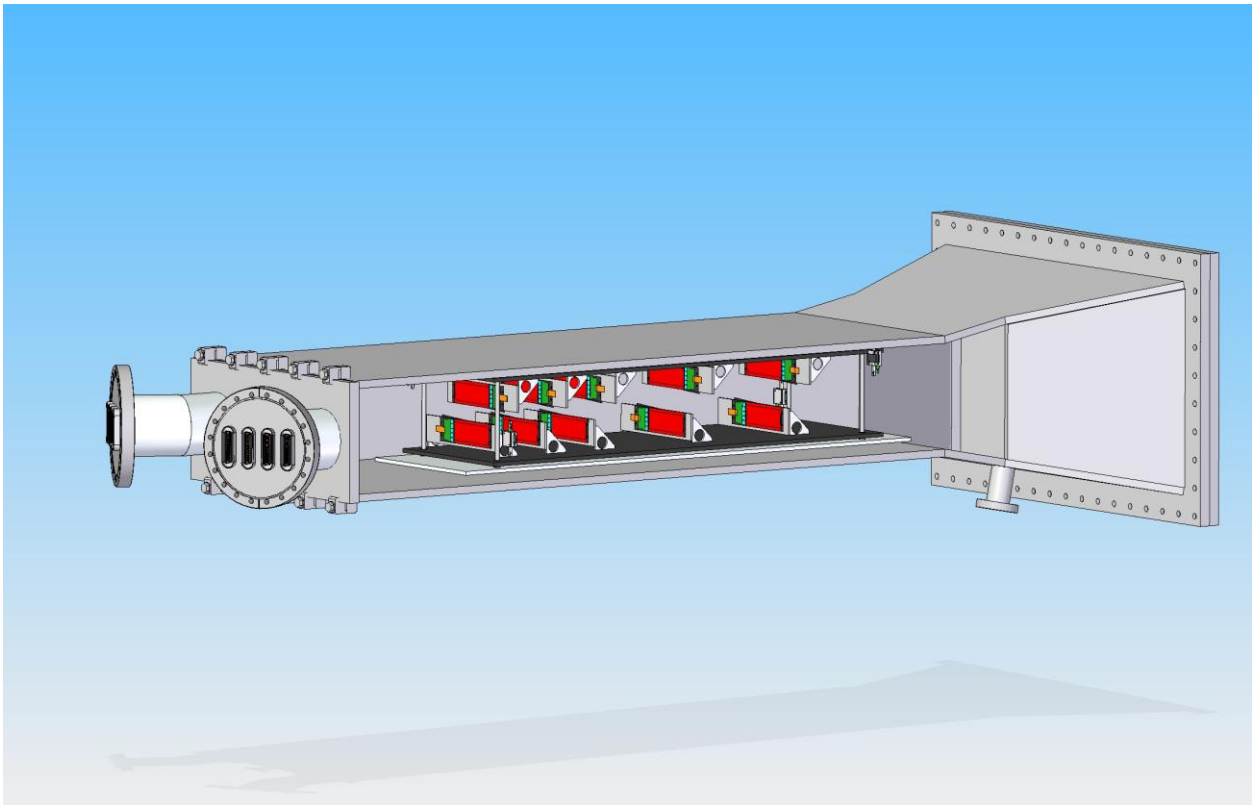

Figure 2.3.6.1: A rendering of the tracker installed inside the existing vacuum chamber from the Hall B TPE analyzing magnet. The new upstream flanges that accommodate connections through the wall of the vacuum chamber are shown at the left.

2.3.7 **References**

1. DØ Collaboration, *DØ Run IIb Upgrade Technical Design Report*, http://d0server1.fnal.gov/projects/run2b/Silicon/www/smt2b/Documentation/D0_Run2b_TDR_Silicon_Sept24_02.pdf

2. M.J. French et al., Design and results from the APV25, a deep sub-micron CMOS front-end chip for the CMS tracker, NIM A 466 (2001) 359–365.

3. P. Azzi et al., *Charge Deposition Model in Silicon*, CDF Internal Note CDF/DOC/TRACKING/CDFR/5080 (1999).

4. M. Friedl et al., Performance of a CMS silicon strip detector module with APV25 readout, NIM A 488 (2002) 175–183

5. Y. Nakahama, Research and Development of a Pipeline Readout System for the Belle Silicon Vertex Detector, University of Tokyo Master Thesis (2006).

6. Panasonic Industrial Products Catalog, http://industrial.panasonic.com/www-data/pdf/AYA0000/AYA0000CE2.pdf

2.4 **Electromagnetic Calorimeter**

The electromagnetic calorimeter (ECal) for the test run will consist of 460 lead-tungstate ($PbWO_4$) crystals with avalanche photodiode (APD) readout. We are planning to use the same crystals that are currently used in the inner calorimeter of the CLAS detector (IC). IC has been operational since 2005 and performed very well in several CLAS experiments. There are no plans to use the IC in the future with the CLAS or CLAS12 detectors. The IC crystals are 160mm long and are tapered. The cross section of the crystal front face is 13.3x13.3mm^2; the cross section of the rear end is 16x16mm^2. Assembled modules (see Figure 2.4.1) that include crystals with Hamamatsu APDs S8664-55 glued onto the rear end and pre-amplifier boards will be used in the construction of the HPS ECal. The IC has 424 modules and there are 38 spare modules on hand.

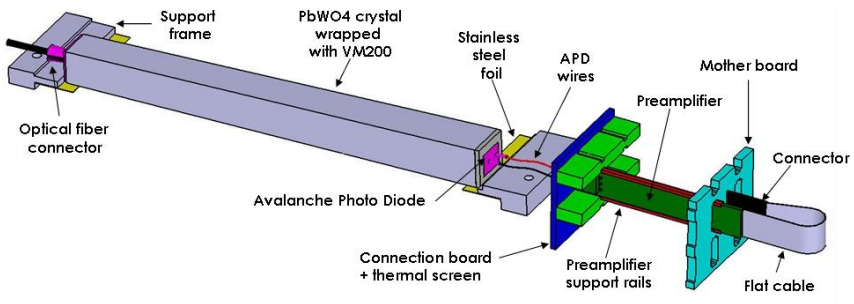

Figure 2.4.1. Schematic view of the IC module. Crystals with APDs and preamplifier boards will be reused for the HPS Test Run ECal. New enclosures with temperature stabilization, support frames, connection boards and mother boards must be fabricated for the ECal.

Crystal modules in the ECal will be arranged in two rectangular formations. There will be 5 layers in each part with 46 crystals in each layer. The ECal will be mounted downstream of the analyzing dipole magnet at the distance of ~137cm from the target. The two formations will be positioned above and below the beam plane such that the edge of the crystal closest to the beam is 20mm from it. There will be a vacuum chamber between the upper and lower formations to let primary and scattered (bremsstrahlung) beam pass through. Figure 2.4.2 is a rendering of the ECal crystal layout together with the vacuum chamber. The vacuum chamber includes openings for the photon and electron beams (displaced because of the analyzing magnet) and additional space to beam's right of the electrons, where radiated electrons will be bent. The calorimeter is separated from the vacuum chamber of the analyzing magnet by a 2 cm thick aluminum vacuum exit window. The primary and scattered (bremsstrahlung) beams go through a continuous vacuum from the vacuum box in the magnet to the ECal vacuum enclosure, which connects to a vacuum chamber leading to the third chicane magnet and beam pipes beyond.

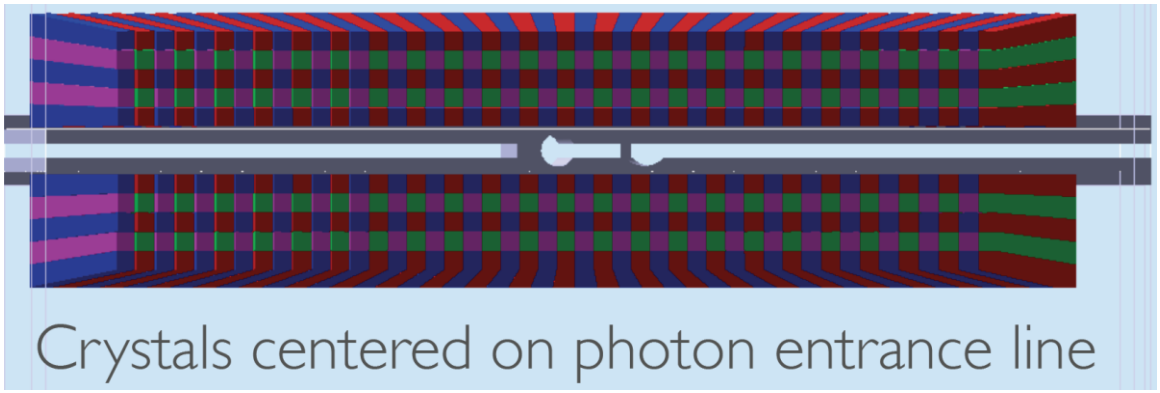

Figure 2.4.2. Beam's eye view of the electromagnetic calorimeter. Colored squares represent lead-tungstate modules. The right side of the gap between ECal parts will be vacuum chamber to allow primary and scattered (bremsstrahlung) beams pass through without interaction. Bigger holes in the support are where the most intense photon (left) and primary electron beam will pass.

2.4.1 **ECal Assembly**

In order to maintain stable performance of the $PbWO_4$ calorimeter, the ECal modules will be arrayed inside a calorimeter box, which provides temperature stabilization at the level of 0.1 ^{0}C (similar to the IC box assembly). The expected energy resolution of the system from operational experience with the IC is $\sigma_E/E \sim 4.5\%/\sqrt{E}$ (GeV).

As in the IC, $PbWO_4$ modules will be connected to a motherboard that will provide power to and transmit signals from individual APDs and pre-amplifier boards. Crystals inside the box will be supported by a carbon honeycomb structure. The.ECal enclosure, crystal supports, connection panels and motherboards are new items which must designed and fabricated.

The CLAS IC box assembly, crystal support frames, pre-amplifier boards, and the motherboard were designed and fabricated by the Orsay (France) collaboration in CLAS. The Orsay group is part of the HPS collaboration and will carry most of the load in the design and part of the construction efforts of the ECal. In Figure 2.4.3 a model of the ECal assembly is shown. Tin the figure, the upstream flange is made transparent to show the front of the crystals and the cross section of the vacuum chamber. Some of the technical details are shown in Figure 2.4.4. The total length of the ECal enclosure is ~40 cm.

A list of new components that must be built or purchased for the ECal is presented below:

- Housing for crystals and the interface made of carbon alveolus, and carbon and/or aluminum inserts

- Support plates made of carbon and aluminum positioned before and after the crystals. These plates provide connectivity to the external environment and transfer the load to the support frame, which has also to be realized.

- Cconnections and supports for the preamplifiers.

- Connection boards, which have two functions: (1) link the APD to the preamplifiers; and (2) thermally disconnect the crystal and preamplifier areas.

- Mother boards, which drive all signals and supply lines. Special tracks for the cables start from the extremity of this component.

- The enclosure which serves as a black box for the photon detector and a thermal shield from the environment is made of insulation and thermal screens cooled at 16°C +/-0.1°C. Thermal stabilization will be accomplished as it was in the IC (Note-RDD_2004_02: Thermal design for the DVCS calorimeter). It is foreseen to design this box somewhat larger than is needed for the Test Run to accommodate the final HPS ECal.

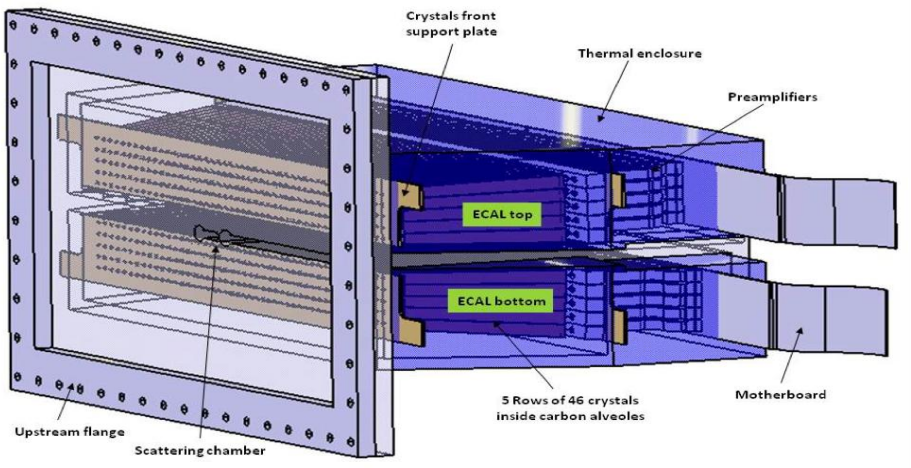

Figure 2.4.3. A conceptual design of the electromagnetic calorimeter.

The design of the ECal is still in a preliminary stage; however the critical items, such as the mechanical stability of the ECal vacuum chamber and the temperature stability of the ECal enclosure, have been thoroughly discussed and addressed.

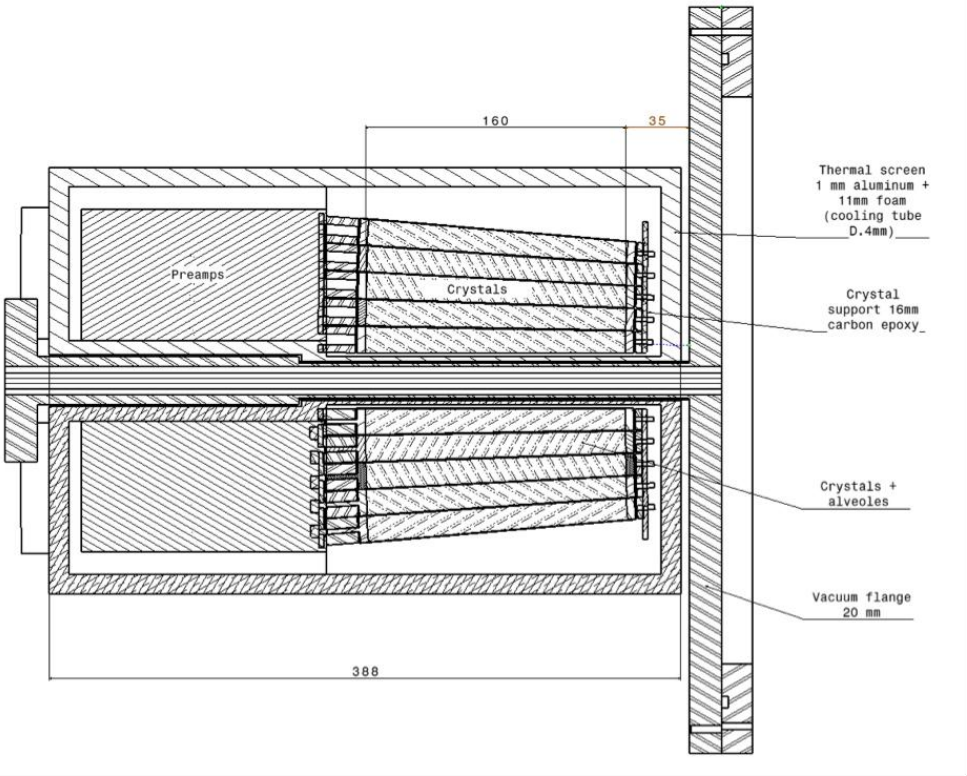

2.4.4. Side view of the ECAL showing the crystals, electronics, enclosure, vacuum chamber, and connection to the flange of the analyzing magnet vacuum chamber. The beam enters from the right..

2.4.2 **Electronics**

Existing low and high voltage systems for the IC will be used for the ECal. In the existing system there are enough spare channels to accommodate the increase in the number of channels to 460. HV and low voltage cables will be needed for the added channels. Connectors on the existing signal cables must be replaced since the layout of the channels will be different.

Signal readout will be done as it was for the IC. Signals from each module will be sent to a signal splitter. One of outputs of the splitter will be fed to a discriminator and then to a TDC channel and to a scaler, while the second one will be sent to a FADC. The trigger from the ECal will be based on FADC information and includes a cluster finding algorithm using FPGA modules. It is described in Section 2.5.1. A similar clustering algorithm was used with the IC, using discriminated signals instead of pulse height information. With FADCs, the energy of clusters will be determined at the trigger level and will be used in making the trigger decision.

2.5 Electronics and DAQ

There are two front-end electronics systems, an Electromagnetic Calorimeter (ECal) system and a Silicon-Vertex Tracker (SVT) system. A level 1 hardware trigger selects events to be read out. Only the ECal provides inputs to the Level 1 trigger system. The triggered events from the two sub-systems are acquired and processed in the data acquisition and processing system. The generic scheme for the HPS DAQ system hardware is shown in Fig.2.5.1.

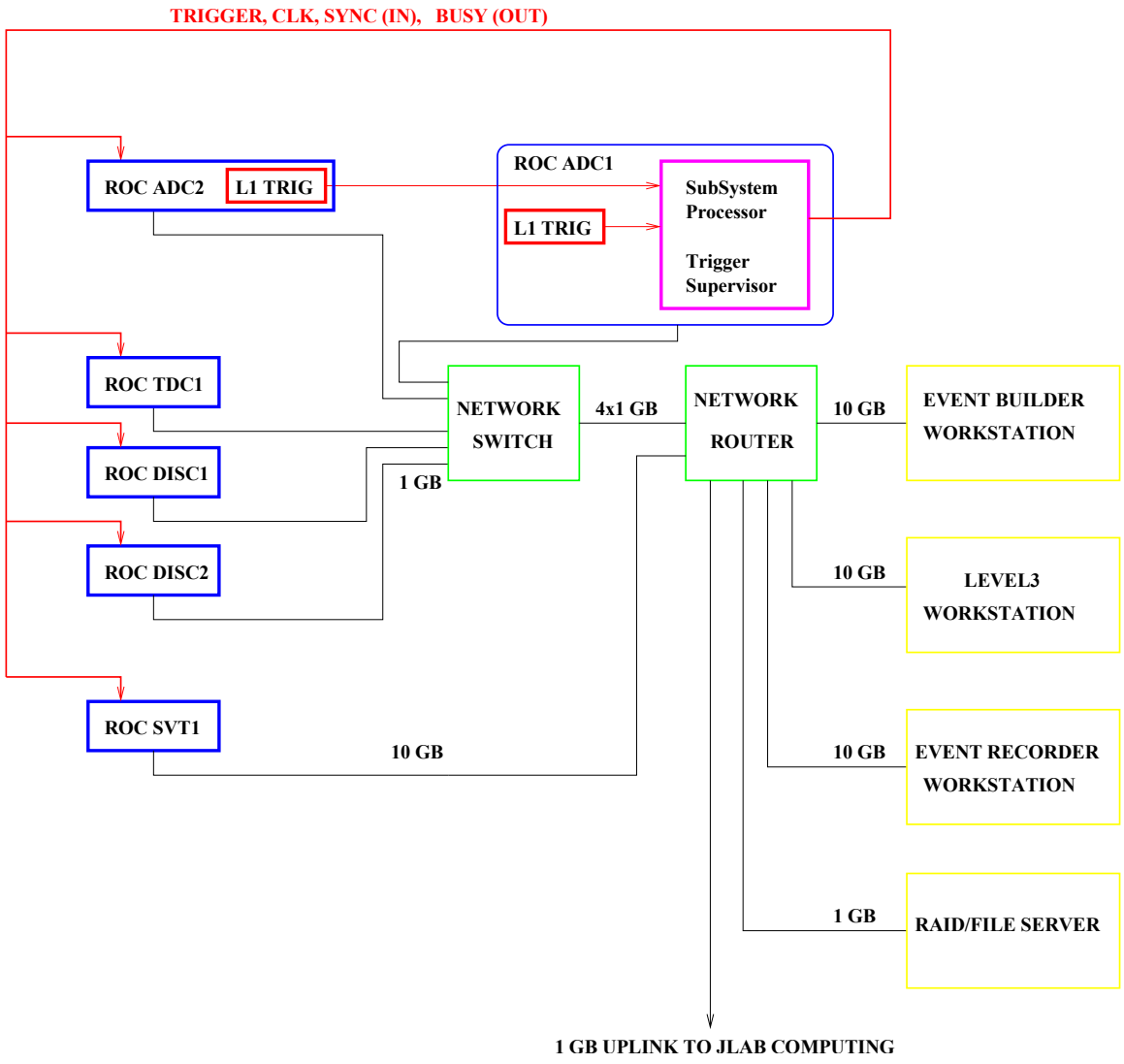

Fig.2.5.1. Readout and processing system block diagram

2.5.1 Electromagnetic Calorimeter Systems

2.5.1.1 Front-end

The Electromagnetic Calorimeter has 460 channels. The system described below can handle up to 496 channels for the ECal. The charge from APD devices is amplified and shaped in existing JLAB front-end electronics as described in Section 2.4. Amplified signals from APDs will be sent to a splitter. The splitter output will feed Flash ADCs (FADCs), scalers and TDCs.

2.5.1.2 Readout

One of the outputs from every splitter channel is connected to a FADC channel packaged in 16-channel VXS modules. Two VXS crates will be used to accommodate 30 16-channel ADC boards, as shown in Figure 2.5.1.1.

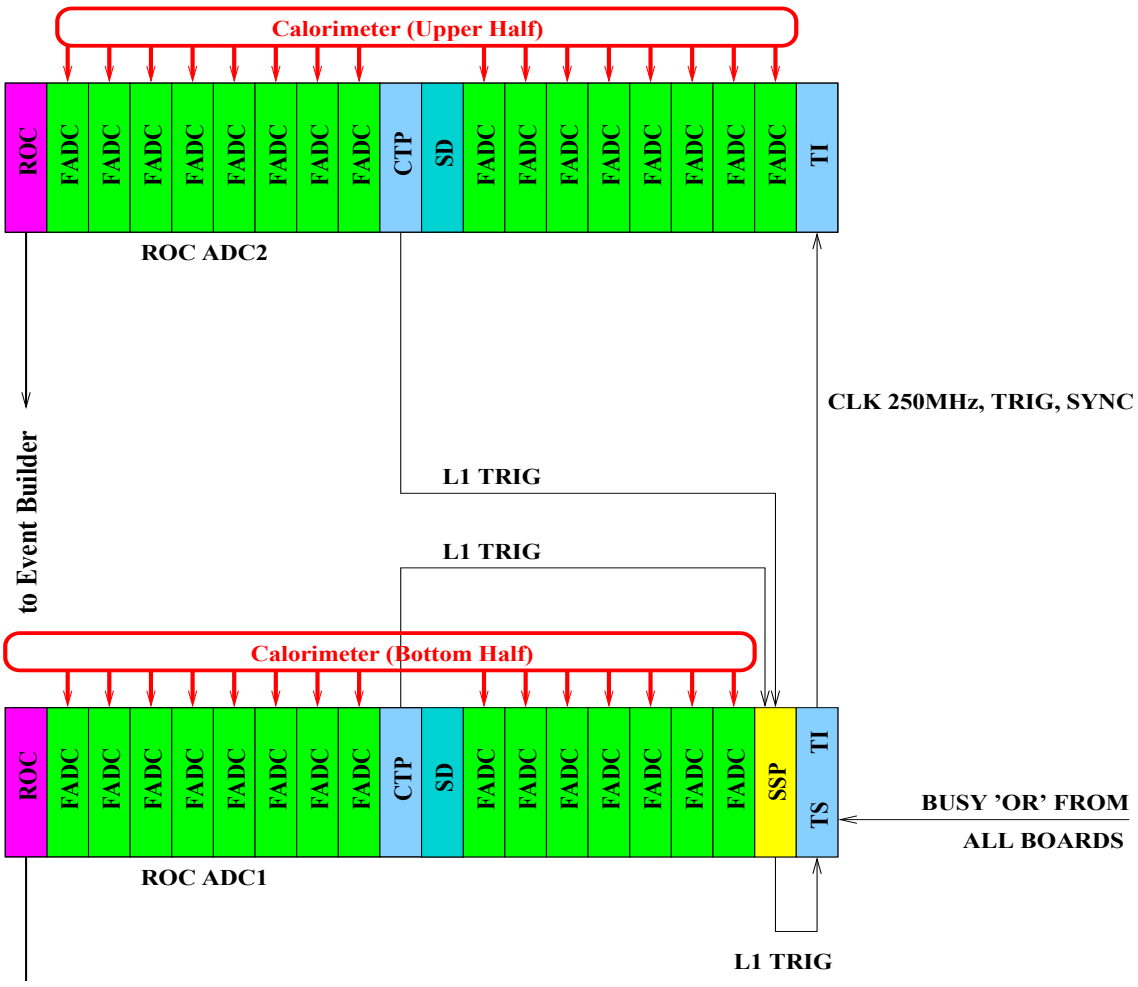

Fig.2.5.1.1 Calorimeter data acquisition and trigger system.

2.5.1.3 **Trigger**

The FADCs are a significant part of the trigger system and will send signal information to the Crate Trigger Processor (CTP) board installed in the same crate. The signal information will include energy for every channel above threshold. A threshold will be applied to the energy sum of several consecutive hits in the same crate. Information will be sent to the CTP board over the back-plane serial bus every 16 ns. The CTP board will perform cluster finding. There are two CTP boards in two VXS crates working in parallel searching for clusters in two parts of the ECal. CTP findings are reported to the Sub System Processor (SSP) board installed in one of the VXS crates. The SSP board forms the final trigger decision.

The 16-channel JLAB-made 12-bit 250-MHz Flash ADC boards are under development and will be in production during 2011 calender year. It is expected that one full crate with FADCs and CTP will be ready for tests for the CLAS12 pre-shower calorimeter in May 2011.

2.5.2 **Silicon Vertex Tracker System**

The SVT readout system is shown schematically in Figure 2.5.2.1.

2.5.2.1 **Front – End Hybrid**

There are a total of 20 silicon strip sensors, each one connected to a hybrid holding five 128-channel APV25 integrated circuits. The APV25 provide amplification and analog storage for trigger accepted events. There are 5 analog outputs for each 640-channel hybrid. Each hybrid will be connected via a multi-twisted-pair cable to a readout board.

2.5.2.2 **Readout**

The SVT readout system is shown schematically in Figure 2.5.2.1. The outputs of up to 10 hybrids are digitized on a ATCA (Advanced Telecommunication Computing Architecture) readout board. The readout board is comprised of a Rear Transition Module-Hybrid (RTM-Hybrid) which accepts signals from the hybrids and connects to the Carrier on Board (COB), a board which fits in the ATCA crate. Each COB carries one Data Transport Module (DTM) and four Data Processing Modules (DPM), which are plugged into it. The hybrids and RTM and DPM are being designed at SLAC for this project; the COB and DTM are boards that SLAC has already developed for use with ATCA. Three ATCA readout boards will be housed in one 14-slot ATCA chassis for the HPS Test Run. The ATCA crate will also be equipped with a commercial CPU board and a custom TI (Trigger Interface) unit to communicate with JLAB DAQ and Trigger Systems. The TI card will also be designed at SLAC, using essentially the same circuit as an existing JLAB VME card but in ATCA format. The TI card is comprised of a Rear Transition Board-Timing (RTM-timing) and a COB with DTM. The data from the readout boards will go over Ethernet to a tracker specific CPU board in the same ATCA crate. This board will process the data and send it in one transfer to the rest of the DAQ system using the CIM card.

The destination host and TCP port will be obtained by the CPU board from run control and passed to all SVT readout boards. Also, the CPU board will propagate DAQ commands (download, prestart, go, end etc) to SVT boards.

The crate also contains an existing 10-G switch card, the CIM (Cluster Interconnect Module) which acts as a switch to connect the 10 readout board, the TI, and the CPU to the JLAB network switch shown in Figure 2.5.1.

The trigger and clock and synchronization signals are received by the TI module and distributed via the ATCA backplane to all the modules.

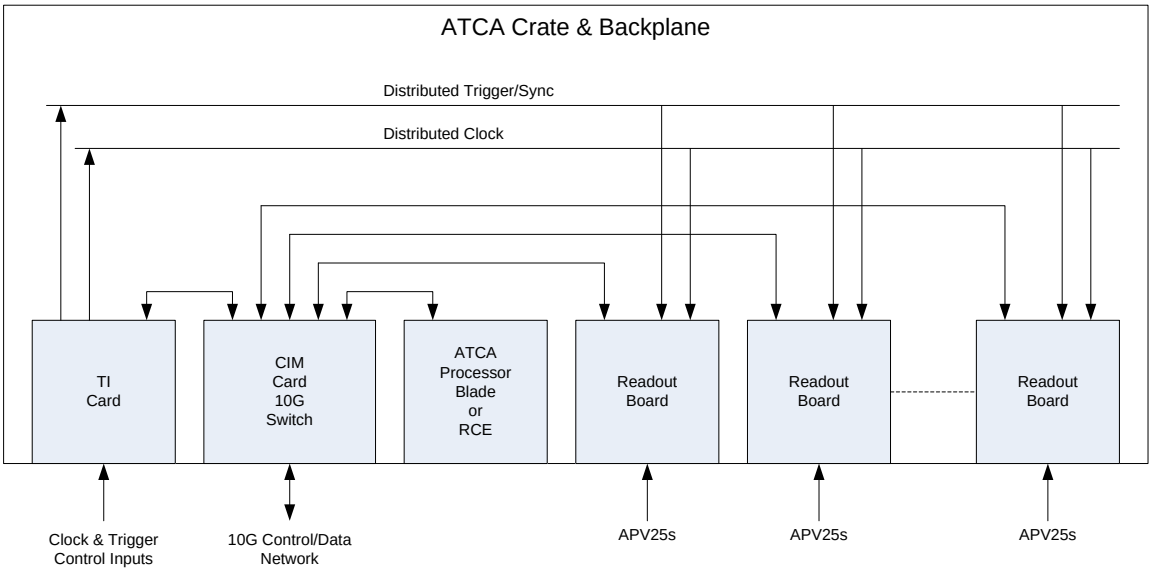

Fig.2.5.2.1. SVT Readout System

2.5.2.3 **Trigger**

The SVT does not provide signals for the Level 1 trigger decision.

2.5.3 **System Timing**

All crates receive the 250-MHz master clock. SVT will divide it by 6 for internal use. The ECal signals are digitized at 250 MHz (every 4 ns) with a trigger signal generated every 16 ns. The phase of the SVT clock will be latched when the trigger signal is received to correct for the phase of the divide by 6 clock compared to the trigger time.

2.5.4 **Level 1 Trigger**

Trigger logic running in CTP boards will search for a coincidence between different signals every 16 ns; i.e., a single trigger operation takes 4 clocks x 4ns = 16ns. The trigger decision made by SSP board will be sent to the Trigger Supervisor implemented as a part of one of the TI

boards. The Trigger Supervisor generates all necessary signals, and controls the entire DAQ system readout through the Trigger Interface units. The Trigger Interface (TI) units installed in every crate participate in the readout process. The system is free-running and driven by a 16 ns global clock with internal FPGA 4 ns clock.

The maximum trigger decision time (latency) is currently set to 3 μs for Level 1. That value is defined by the SVT readout APV25 chip. A preliminary FPGA algorithm analysis shows that 3 μs for Level 1 should be enough to complete cluster finding, energy reconstruction, and energy selection in the ECal.

2.5.4.1 Trigger Rate

The maximum trigger accept rate is 50 KHz.

2.5.4.2 Occupancy and Number of Samples for each Trigger

The assumption is that the tracker system will run at 3 times the noise threshold. The occupancy is thus 0.135%. The above occupancy results in 17 SVT channels over threshold. Background studies show the average track multiplicity in an event is 10. On average, each track produces two "hit" strips in each of the two detectors constituting a layer. So there are 10(tracks) x 2(strips/track) x2 (detectors/layer) x 5 (layers) = 200 samples. Adding the noise pulses gives 217 samples. Each of these channels over threshold results in 6 digitized values, which record the pulse heights in time bins adjacent to the hit in question, for subsequent pulse shape reconstruction and timing. Thus an average event has 217 x 6 = 1302 samples for each level 1 trigger signal.

2.5.5 Trigger Deadtime

The proposed trigger system is nearly deadtimeless. The trigger decision goes to the Trigger Supervisor every 16ns. The Trigger Supervisor can apply deadtime if necessary, for example on 'busy' or 'full' condition from the front end electronics. There is a limitation on the FADC board on the number of triggers received within a short time interval. For example, if four triggers arrived during about 200ns then the FADC will stop receiving new triggers until at least one of four is processed. We are not expecting to hit that limitation with our expected event rate ~50kHz.

2.5.6 Dataflow

2.5.6.1 SVT Data Rate and Volume

The amount of data for a ~40 MHz clock and a 50 KHz rate (APV25) is estimated as:

- Structure

- Each chip 12-bit header (3 start, 8-bit address, 1 error) plus 10 bits/channel if 10-bit ADC is used
- For each ASIC need additional 9 bit chip address

– Number of bits for each hit
- 9-bit chip address (16-bit)
- 12-bit header (16-bit)
- 6 times 10-bit ADC value (72-bit) (assume 10-bit ADC for now since need bare minimum 8 bits)
- 13 bytes (104 bits) (81 bit minimum)

– Data volume and rate
- 217 ASICs x 2 bytes chip address: 434 bytes
- 217 hits x 2 bytes header: 434 bytes
- 217 hits x 6 samples x 1.5 bytes: 1953 bytes

The resulting data rate is 2821 bytes x 50 KHz = 141.1 Mbytes/sec.

2.5.6.2 **ECal Data Rate and Volume**

A single FADC event contains 8 bytes of header for each FADC board, plus 4 bytes per accepted hit (hit means here integral over entire pulse).

With an estimate of 10 % acceptance rate, for each 16-channel ADC board that results in 8 bytes plus 1.6 x 4 bytes = 14.4 bytes average. At a trigger rate of 50 KHz the data rate is then 720 kbytes/sec for each board. A crate holding 16 FADC boards produces 11.5 Mbytes/sec. The limitation will be at the level of 50MB/s data rate from each VXS crate, so there is adequate headroom.

The total data rate from the ECal consisting of 35 FADC boards is 35 x 14.4 bytes x 50 KHz or 25.2 Mbytes/sec. (The total acceptance rate assumed is 10% of 640 channels or 64 channels for each trigger).

2.5.6.3 **Event builder**

The event builder is a program running on a server assembling the calorimeter, tracker, and muon data into complete events belonging to the same trigger event

2.5.7 **Monitoring and Calibration**

Four practically independent monitoring systems are currently used in JLAB: Nagios-based computer and network monitoring, SmartSocket-based DAQ and Online monitoring, EPICS-based slow controls monitoring, and data monitoring. In addition, a few smaller hardware-

specific systems are used. The data monitoring system includes visualization only with almost no alarm capabilities.

2.5.8 **Readout Controllers, Computing and Network**

Readout Controllers (ROCs) are installed in every VME, VME64X, VXS and ATCA crate. The ROCs are collecting data from the front-end boards, processing it and sending it to the Event Builder over the network. Currently mvme6100 controllers with a prpmc880 or pmc280 co-processor modules are employed. That configuration is fast enough to meet the HPS requirements. By the time of HPS startup, a new generation of multi-processor and multi-core ROCs will be available. ATCA crates will be equipped with commercially available multi-core CPU module.

A Foundry Router is currently used as the backbone of the DAQ system, providing 1GBit and 10GBit connections between components and to the JLAB Computer Center. The Event Builder, Event Recorder, and other critical DAQ components are running on 4-CPU Opteron-based servers, and that configuration is sufficient for HPS as well. ROCs are linked to the Foundry Router through smaller 1GBit switches with 4GBit uplinks. The HPS data storage system (RAID5) is sufficient for up to a 100~MByte/sec data rate.

3 Simulated Detector Performance

3.1 Trigger Simulations

The decision to process recorded data in ADCs and TDCs will come from a fast analysis of clusters and hits in the ECal by a Level-1 trigger processing system. Details of the Level-1 trigger electronics and organization were presented in the previous section. Here we discuss the trigger algorithm and the expected Level-1 trigger rate based on GEANT-4 simulations of the detector.

The test run will be looking at (e^+e^-) final states. The level-1 trigger algorithm will search for two clusters of energy in opposite segments of the ECal (with respect to the beam direction), since the heavy photon is produced predominantly in the direction of the beam and thus pairs of oppositely charged leptons will be well separated in opposite segments of the ECal.

The Bethe-Heitler process will generate most of the electron pairs, however, due to high rates (high accidental coincidences) and overlapping phase space, processes such as elastic scattering, photon bremsstrahlung and Moller scattering will contribute in the trigger (accidental final states (γe^-) and (e^-e^-)). The coincidence time used by the clustering algorithm for grouping hits in individual counters into clusters will play a crucial role in reducing the trigger rate.

3.1.1 GEANT-4 simulations of the ECal

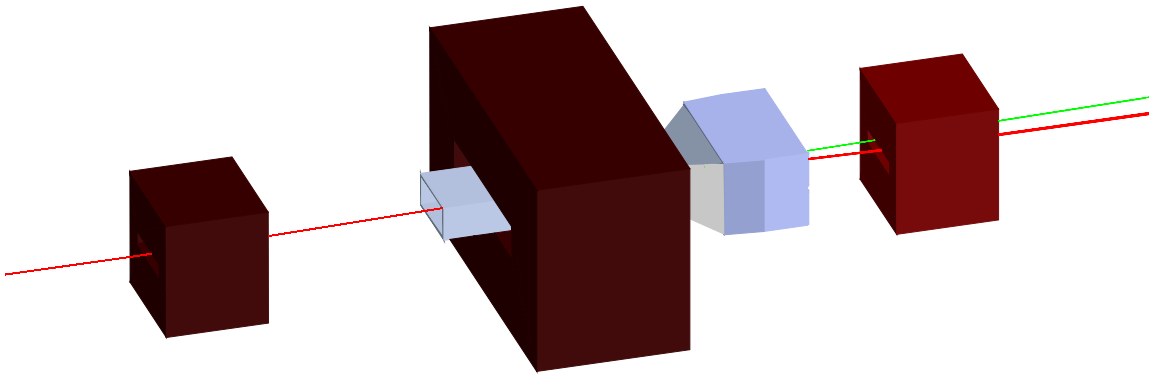

Figure 3.1.1.1 Rendering of the GEANT4 simulation showing the three magnets in red and in gray the vacuum box for the silicon tracker system and the enclosure for the electromagnetic calorimeter. The red line represents the electron beam, the green line represents secondary photons produced in the target.

For the study of the calorimeter and the trigger, a full GEANT4 model of the experiment was initiated. This model is described in more detail in the PAC proposal. The test run makes use of the same GEANT4 engine with a modified geometry, reflecting the modified setup of the test run.

All the key elements of the experiment are implemented in the model: the two steering magnets ("Frascati magnets") and main analyzing magnet, the target, the silicon trackers, the main components of the vacuum system, and the electromagnetic calorimeter. For studying the beam properties all the magnetic fields were modeled using a measured field map. For large statistics running the fields were uniform fields, tuned to reproduce the beam path of the mapped field version. Figure 3.1.1.1 shows a rendering of the test setup.

The electromagnetic calorimeter (Ecal) will consist of 5 rows of 46 lead-tungstate crystals for each of the top and bottom halves of the detector. The Ecal is separated from the beam vacuum by a 2 cm thick aluminum vacuum exit window (made transparent in the figures). The beam goes through a continuous vacuum from the vacuum box in the magnet to a vacuum enclosure made from 1 cm aluminum plates, which is inserted between the top and bottom calorimeters. To further reduce the background rates without diminishing the structural integrity, a small area circular and oval region of the aluminum plates is cut out where the most intense part of the photon and electron beam respectively, exit to the beam dumps. These holes were carefully aligned and angled so that they are centered on the actual photon and electron beams. A rendering of the simulated calorimeter is shown in Figures 3.1.1.2 and 3.1.1.3.

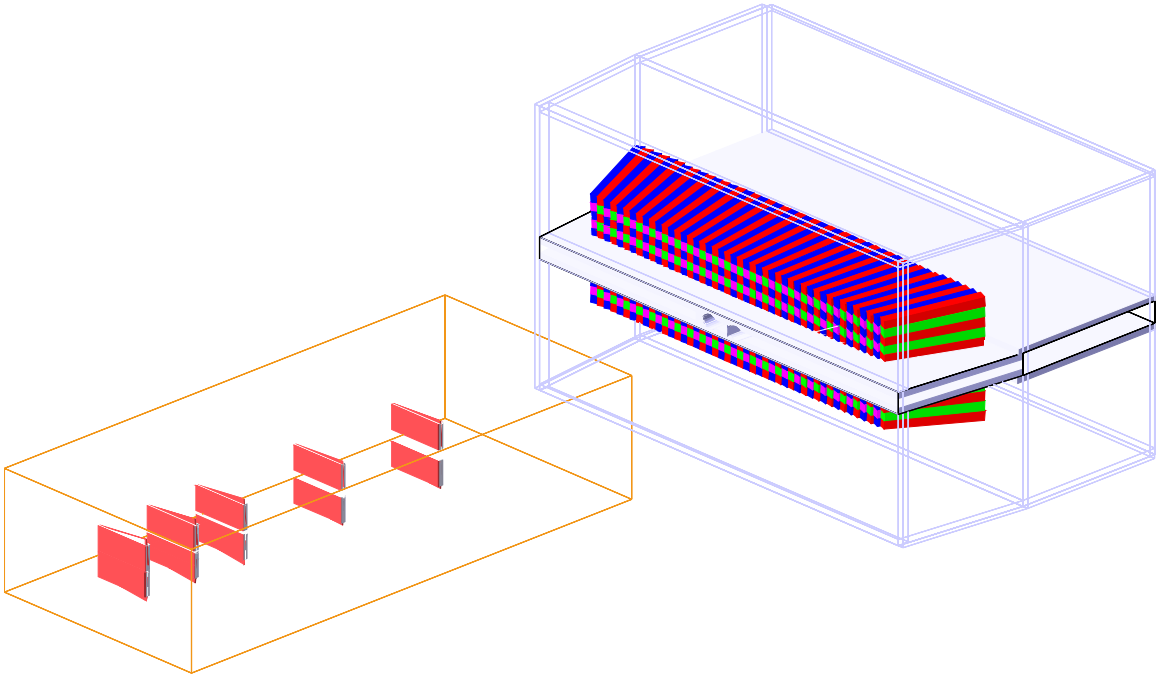

Figure 3.1.1.2. Rendering of the detector simulation used for trigger studies. The orange box represents the container for the silicon trackers (outlined only), the red rectangles represent the silicon tracking layers, and the larger blue-gray outlined rectangles represent the box for the calorimeter. The final object shows the calorimeter, with the crystals colored in alternate colors for clear visibility.

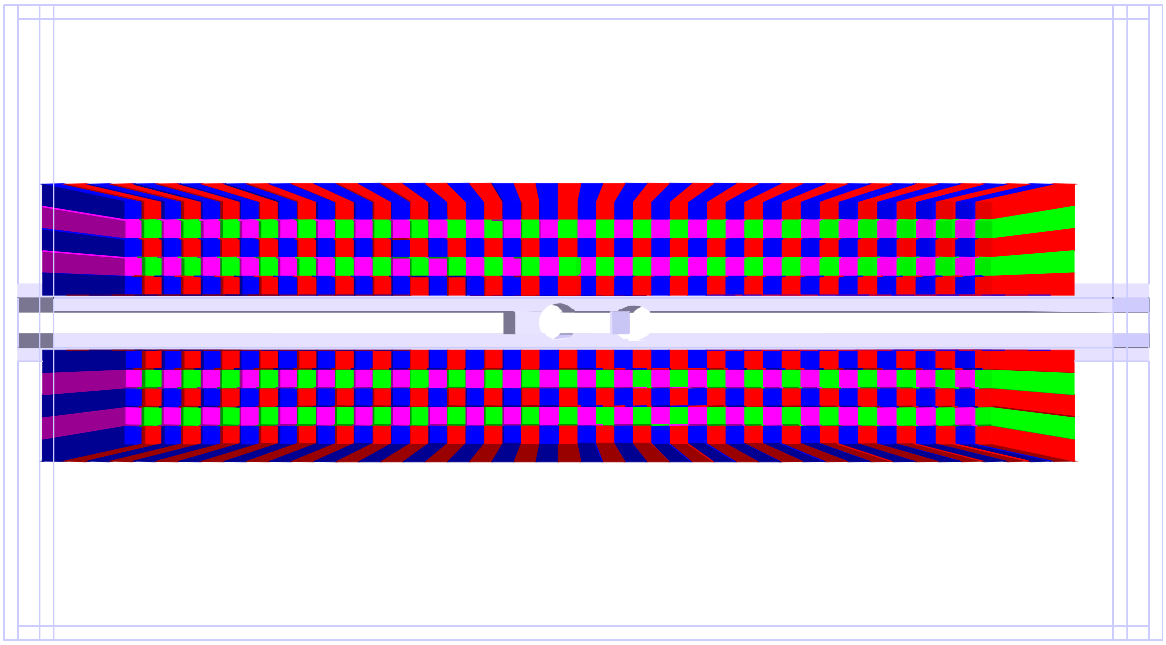

Figure 3.1.1.3. A rendering of the electromagnetic calorimeter setup looking down the beam line. The front exit window and side plates are rendered transparent to permit a view of the crystals and the vacuum plates.

To study the performance of the calorimeter and the trigger logic a large number of background events were simulated. Background events were generated by sending 5,000 2.2 GeV electrons through the 0.125% X_0 tungsten target (equivalent to 4ns of a 200 nA beam) and letting the GEANT4 physics models generate the expected backgrounds (scattered electrons, produced photons and other particles). The physics models used in this simulation include all electromagnetic and hadronic processes implemented in GEANT4. To simulate longer integration times, several events were added together. Validity of this summing method has been verified with the simulations performed for the HPS proposal.

For the trigger studies, input events were used that were generated with MadGraph/MadEvent. These events simulated A' masses of 25, 50, 75, 100, 150, 200, and 250 MeV/c^2. The output files of these simulations could be merged with the background simulation output files to create realistic data samples for different scenarios.

3.1.2 **Calorimeter Performance**

Two aspects of the calorimeter performance were studied with the simulation. The hit rates on the individual crystals were looked at to make sure these rates will be within a reasonable range for the expected running conditions, and the expected trigger rates for simulated A' particles and for background events were studied to make sure they do not exceed the maximum allowable DAQ trigger rate. This section details the hit rates, the next section the trigger rates.

As one would expect, the highest rates occur on the crystals that are closest to the exiting electron beam. A map of the percentage of events with at least one hit, the hit occupation, for each crystal, using a time integration window of 8 ns and a hit threshold of 100 MeV, is shown in Figure 3.1.2.1. The maximum hit occupation occurs for crystal number -4 and -3 in the first row,

with close to 25% occupancy. To further decrease the rates on the crystals it will be possible to set the threshold even higher for individual crystals.

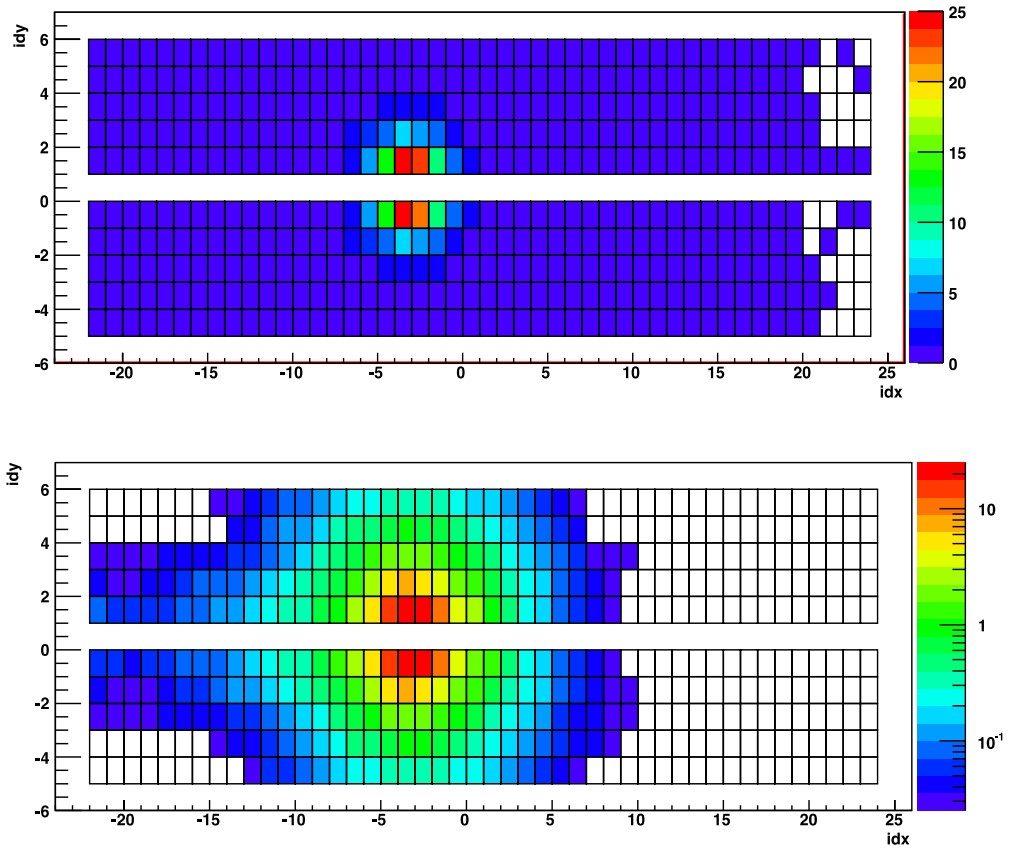

Figure 3.1.2.1 Hit occupancies in the electromagnetic calorimeter for a time window of 8 ns and a threshold of 100 MeV. The figure on the top has a linear z-scale, the figure on the bottom is identical except for the logarithmic z-scale. Note that the x and y axis are the index of the crystal, not the position. The increased threshold reduces the occupancies on the hottest crystal (# -4 and -3 row 1) to around 25%.

A more detailed picture of the running conditions for the crystals of the electromagnetic calorimeter can be obtained by looking at the hit multiplicities, the number of hits in a specified time window with energies above some threshold. Figure 3.1.2.2 shows the multiplicity for crystals in row 1 and a time window of 32 ns, with a threshold of 100 MeV. The y-axis indicates the number of hits in an event with the specified time window, and the color indicates the percentage of the events where the crystal had that many hits, thus a sum over a column of the histogram adds up to 100%. One can see that for a threshold of 100 MeV and a time window of 32 ns, crystals numbered between number -5 and -2 have 1 hit per event for 30 to 40% of the time and two hits for up to 20% of the time. A plot of the projection on to the y-axis for crystal -4 is shown in Figure 3.1.2.3 (light blue line of left panel.) This figure illustrates how reducing the time window reduces the multiplicity on the crystal, exactly as expected. At a threshold of 100 MeV and time integration windows shorter than 16 ns, the multiplicities on the hottest crystal are reasonable, less than 8% of the events. The right side plot of Figure 3.1.2.3 shows the rates for different thresholds for the crystals in the first row. Crystals in the hottest region will need to run with an increased threshold.

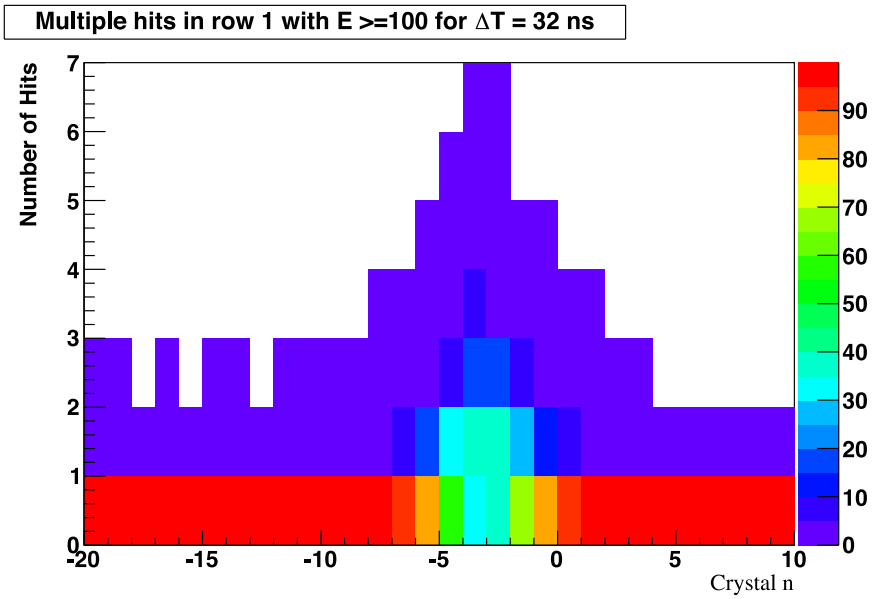

Figure 3.1.2.2 Hit multiplicities for the first row of crystals around the area of the beam exit for a threshold of 100 MeV and a time window of 32 ns. The y-axis shows the number of hits in the time window, the z-axis (colors) shows the percentage of events with this hit occupancy. For only the hottest crystals there is a significant probability of getting a double hit.

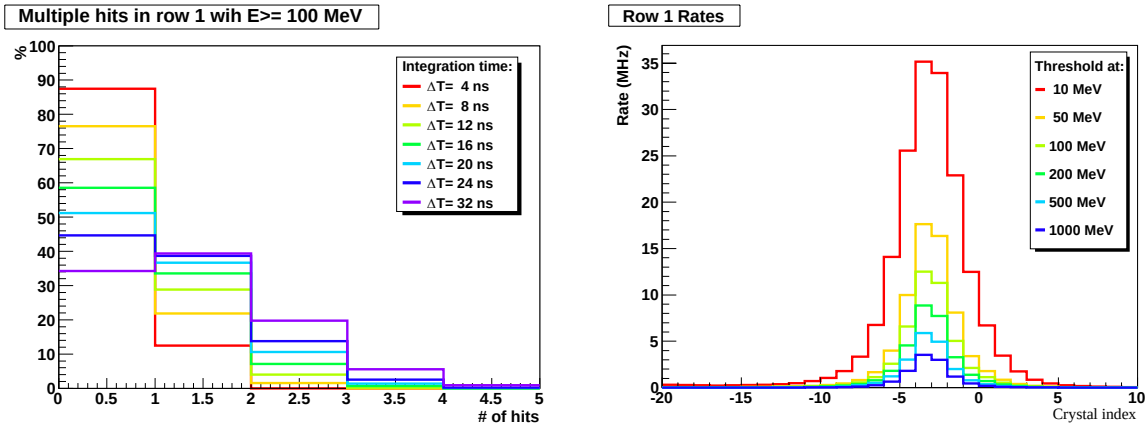

Figure 3.1.2.3. Left: projection onto the y-axis of the multiplicities of figure 5 for crystal number -4. and similar projections for shorter time windows. Right: hit rates for crystals in the first row for different thresholds.

3.1.3 **Level 1 trigger simulations**

To accurately estimate trigger rates, a Level 1 trigger algorithm was developed and optimized using simulated background data and simulated A′ events with masses ranging from 25 MeV/c^2 to 250 MeV/c^2. The events were processed with the full GEANT4 based simulation described in the previous section. For the background events, two simulated 4 ns events at 200 nA were summed to simulate a single 8 ns event. This allowed for the simulation of background events with a trigger coincidence window of 8 ns.

To accomplish the short coincidence timing, the Crate Trigger Processor (CTP) will run in a modified mode. In the standard operational mode, with a predefined integration time and delay,

the time of the hit reported to the CTP will have about 16 ns jitter. With a 16 ns time resolution for each channel, a reasonable minimum time window for triggering cannot be less than 32 ns (2 trigger time buckets). To shorten the trigger time window the CTP can use 6 bits for the energy sum (FADC sum), instead of the standard 8 bits, leaving two remaining bits of an 8 bit word to determine the 4 ns clock cycle when summing started. In this arrangement, time jitter at the CTP for each channel will be 4 ns and the coincidence time between channels can be reduced to two 4 ns clock cycles, 8 ns. Differences in signal propagation times between channels can be accommodated using internal delays in CTP (with 4 ns steps).

The first step in the Level 1 trigger algorithm is the identification of clusters in the electromagnetic calorimeter. A very simple cluster finding algorithm was used which maximized the number of clusters that would be found. The cluster finding algorithm followed the following logic steps:

1) For each hit in the calorimeter with at least 50 MeV of energy,
2) Search the 3x3 square around the hit for other hits (smaller regions for hits on borders).
3) If a hit with more energy is found, the original hit is not the cluster center,
4) Else add up the energies of the hits over threshold of 30 MeV, in the 3x3 square if these hits were within 8 ns of the center hit.

The resulting cluster samples were then studied to define the most effective trigger, for which the criteria are the largest acceptance of simulated A′ events and the highest rejection of background events. Thus the ratio of accepted A′ events to background events was maximized, with the additional constraint that the background trigger rate would not exceed 30 kHz.

Table 3.1.3.1 shows each of the subsequent cuts and their effect on the number of accepted A′ trigger candidates together with the effect on the background trigger candidates. The simulated A′ mass used was 75 MeV. Numbers are given as a percentage of the total number of simulated events. A more detailed description of each trigger selection cuts follows.

At the lowest level, a trigger required two good clusters in opposite quadrants of the calorimeter. Many events would have multiple clusters in at least one of the two quadrants, in which case all combinations of clusters were tried for trigger candidates. This double counting is not shown in the first row of the table, and eliminated in the last step. This accounts for the increase from the first to the second row in the table.

Trigger Cut.	75 MeV/c^2 A′ Acceptance	Background Acceptance	Background rate
Events with least two opposite clusters	49.4%	3.55%	4.4 MHz
Cluster energy > 100MeV and < 1.85 GeV	70.8%	2.43%	3.0 MHz
Energy sum <= E_{beam}*sampling fraction	66.4%	1.15%	1.4 MHz
Energy difference < 1.5 GeV	66.3%	0.95%	1.2 MHz
Lower energy - distance slope cut	57.8%	0.11%	138 kHz
Clusters coplanar to 35°	57.2%	0.051%	63 kHz
Eliminate crystals -5,-4,-3,-2,1,2	52.0%	0.020%	25 kHz
Not counting double triggers	38.3%	0.018%	22.5 kHz

Table 3.1.3.1.Trigger selection cuts and their effect on the A' acceptance and background rate, as a percentage of the total number of simulated events. An A' mass of 75 MeV/c^2 was used for this illustration.

As the table shows, a large fraction (3.55%) of the background events have at least two clusters in opposite quadrants of the detector. This would correspond to a background trigger rate of 4.4 MHz. A further refinement on the trigger conditions requires that each of the clusters has an energy of at least 100 MeV, but no more than 1.85 GeV. This eliminates low energy background hits and hits from electrons with energies close to the beam energy, while having little effect on the A′ acceptance. (Note that in the table the counting of the double triggers give the false impression that the acceptance is higher after this cut.) The fraction of accepted background events now drops to 2.43% (3 MHz). The algorithm now identifies the more energetic and less energetic hit which make up this trigger pair and requires that their sum is less than the beam energy multiplied by the calorimeter sampling fraction (in this case 2 GeV). This cut removes some of the pileup and accidental events. A further cut requires that the two hits do not differ in energy by more than 1.5 GeV. These cuts reduce the background acceptance to 0.95% (1.2 MHz).

Next a two dimensional cut is made in distance (of the hit from the beam) plane versus the energy (of the hit). These distributions are shown in Figure 3.1.3.1. The previously mentioned lower energy cut for the clusters is shown as the vertical black line. The histograms show that an additional cut for the least energetic cluster along the red sloped line (E + d 3.2 (GeV/cm) < 800 MeV), effectively eliminates background events, reducing the background acceptance to 0.11% (138 kHz).

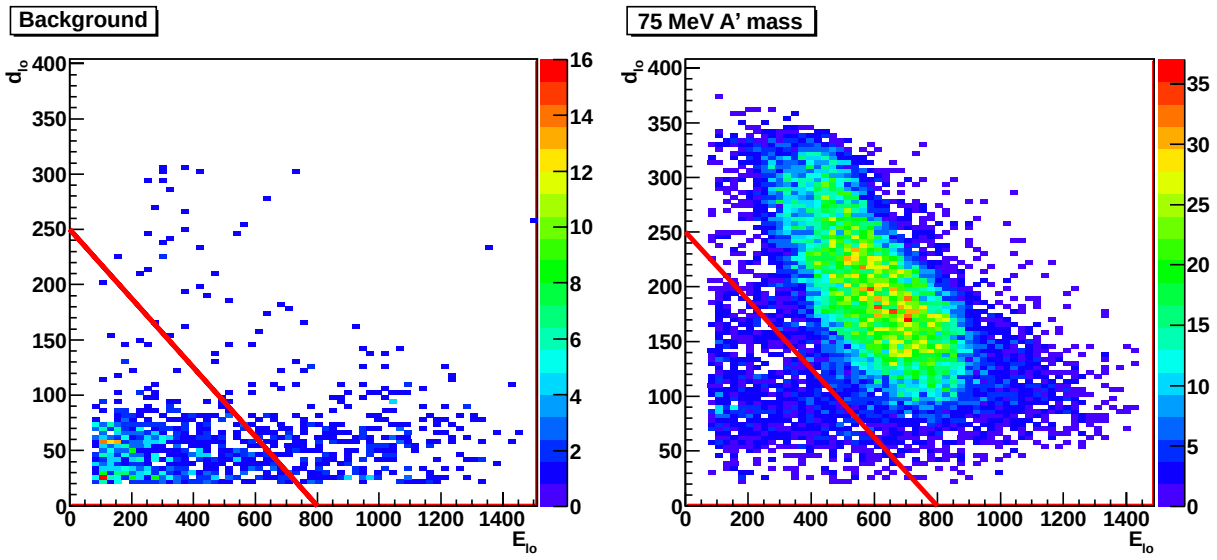

Figure 3.1.3.1. The distance of the cluster center to the beam is plotted versus the energy of the cluster for the less energetic cluster of the trigger pair. The left side plot shows background events, the right side plot shows simulated A' events with a mass of 75 MeV/c^2. As can be seen from the plots, an effective cut to eliminate background events without significantly affecting the A' acceptance is indicated by the red lines.

The requirement that the two clusters are coplanar with the beam within 35 degrees further eliminates background events, leaving 0.051% (63 kHz). Eliminating a few "hot" crystals from the trigger cuts the background rate down further to 0.02% (25 kHz). Finally, removing the remaining double triggers reduces the background acceptance to 0.017 % or 22.5 ±1.3 kHz.

These cuts leave us with a trigger rate of close to 25 kHz, which is acceptable to the trigger electronics, which has a maximum rate of 50 kHz. It still leaves some headroom for less than perfect beam conditions, a slight increase in the beam current, or inaccuracies in the GEANT4 physics model. If an additional reduction of the trigger rate is desired, it is possible to remove a few more crystals from being considered for the center of a cluster.

The same trigger algorithm was run on simulated data for a number of different A' masses. The resulting acceptance estimates are shown in Table 3.1.3.2 and Figure 3.1.3.2. The proposed trigger algorithm retains high efficiency for signal events and suppresses the background triggers by a factor of 100.

A' Mass (MeV/c^2)	25	50	75	100	150	200	250
Ecal	6.5%	29.2%	38.3%	33.9%	16.8%	7.6%	4.2%

Table 3.1.3.2. Trigger acceptance estimates for different A' masses for runs with a beam energy of 2.2 GeV.

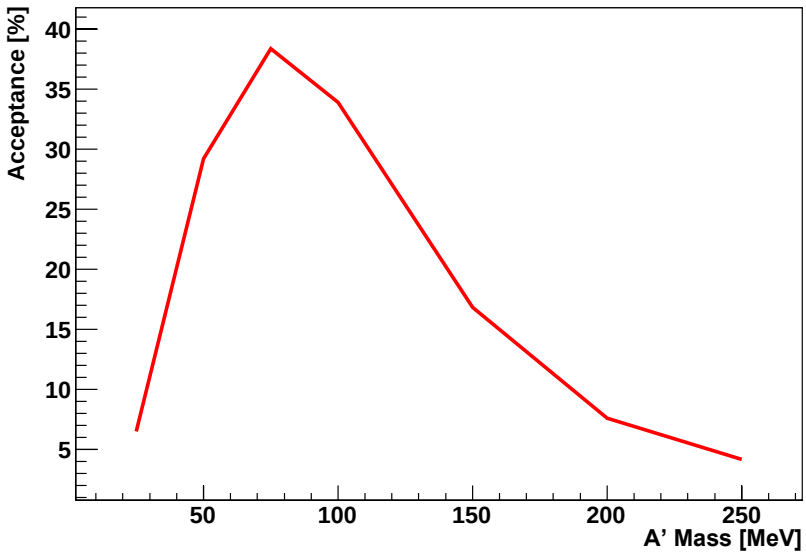

3.1.3.2. Trigger acceptance estimates for different A' masses for runs with a beam energy of 2.2 GeV.

The GEANT4 physics models do not include the radiative and Bethe-Heitler trident processes. Although these trident processes have a large cross section, a large fraction of events do not satisfy the trigger conditions either because electrons/positrons are produced in a small polar angle or the energies are soft. We estimate that these processes will contribute less than 8 kHz to the overall trigger rate, resulting in a total trigger rate less than 30±1 kHz.

3.2 **Tracker Occupancies and Acceptance**

Figure 3.2.1 shows the distribution of charged particle hits in Si tracker layer 1 which is located 10 cm from the target as generated by EGS5. The beam energy is 2.2 GeV, and the target thickness is 0.125% X_0. Multiple Coulomb scattered beam electrons are confined within 0.5 cm of the beam axis (x=y=0), while the low energy Moller electrons are distributed in a parabolic shape. There are very few positrons. From these distributions, the detector occupancy in the horizontal Si strip sensor in the 7.5 ns time window is calculated for a 200 nA beam current and five different target thicknesses, 0.25% X_0, 0.125% X_0, 0.10% X_0, 0.075% X_0, and 0.05% X_0, and is shown in Figure 3.2.2. As described in Section 4.3.4, the dead zone is defined by using a criterion that the maximum occupancy in Layer 1 is 1%. For a 0.125% X_0 target and 200 nA beam, the occupancy is 1% at a distance of 1.5mm from the beam in Layer 1, which corresponds to a dead zone of ± 15 mrad. As long as the product of target thickness (T) and beam current (I) is constant, the same A' production rate is maintained. Since the multiple scattering and hence the effective beam size is reduced in a thinner target, it is advantageous to use a thinner target and a higher current. Using the constraint that the occupancy is 1% at 15 mrad, we find the beam current I which gives this occupancy for each of several potential target thicknesses T. The quantity $(I \cdot T)^{1/2}$, which is approximately proportional to the sensitivity $S/\sqrt{B}$, is given in Table 3.2.1, showing how the sensitivity improves as the target thickness decreases.

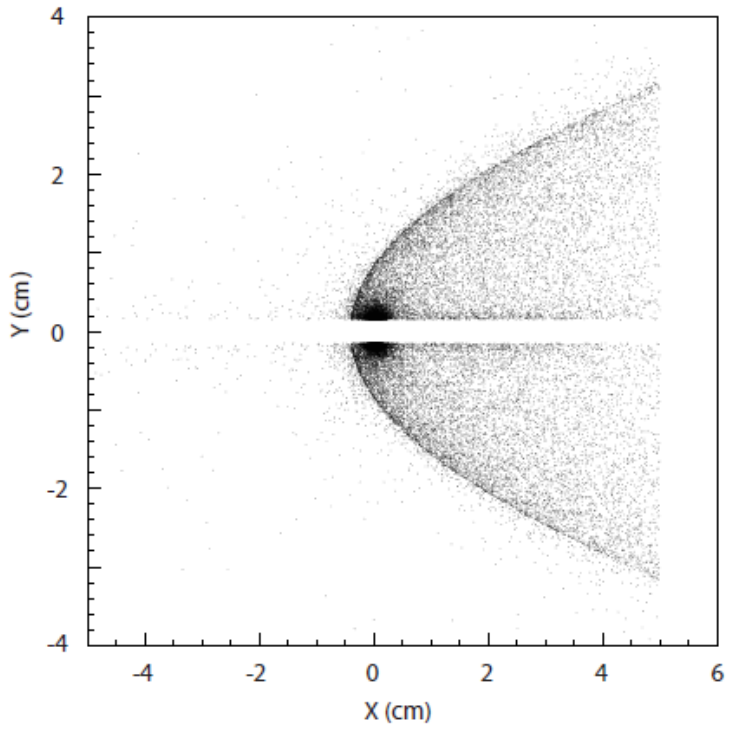

Figure 3.2.1 Charged particle distribution in layer 1

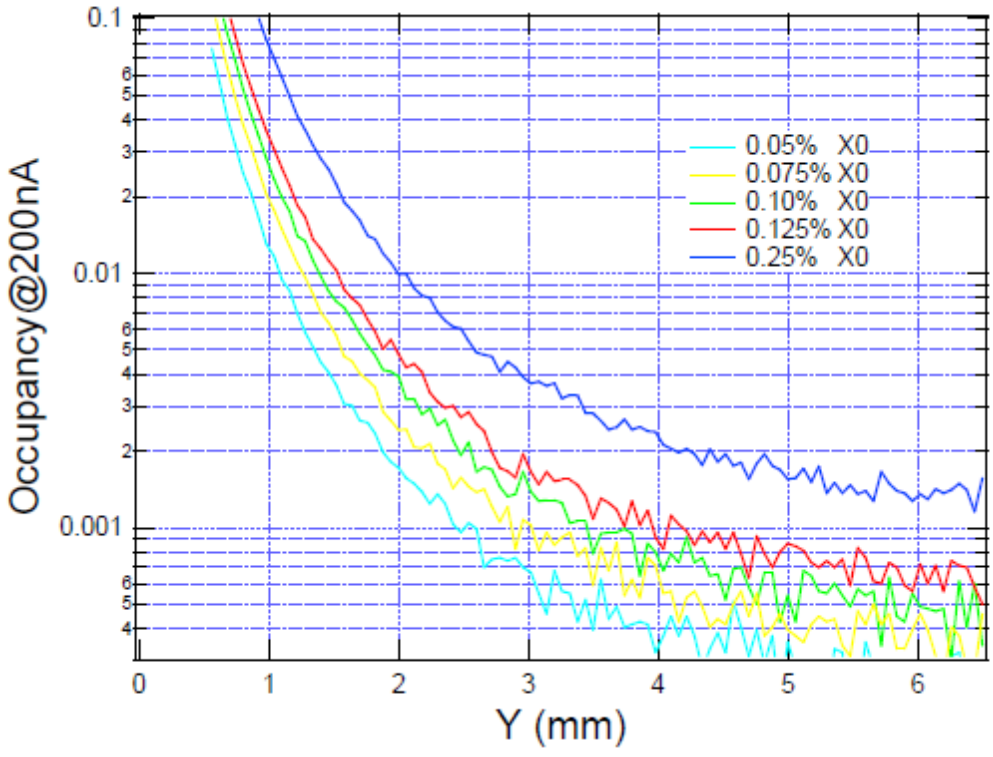

Figure 3.2.2 Silicon sensor layer 1 occupancy at 200 nA vs distance from the beam in mm.

Target thickness (% X_0)	Beam Current (nA)	$\propto S/\sqrt{B}$
0.25	85	9.2
0.125	190	13.7
0.10	250	15.8
0.075	340	18.4
0.05	530	23.0

Table 3.2.1. Beam current yielding 1% occupancy in Silicon sensor layer 1 for various target thicknesses at 2.2 GeV, and the relative experimental sensitivities which result.

Once the dead zone is determined, the tracker acceptance can be calculated by requiring that both e+ and e- from A′ decay are detected in all ten silicon layers. The tracker parameters given in Table 2.3.4.1 are used. Figure 3.2.3 shows the tracker acceptance as a function of A′ mass at beam energy of 2.2 GeV when the A′ decays at the target. The tracker has useful acceptance from 20 MeV to 250 MeV; lower (higher) beam energies can probe A's of lower (higher) mass. At the lower mass side, the dead zone limits the acceptance, while the transverse tracker size limits the acceptance at the higher mass side.

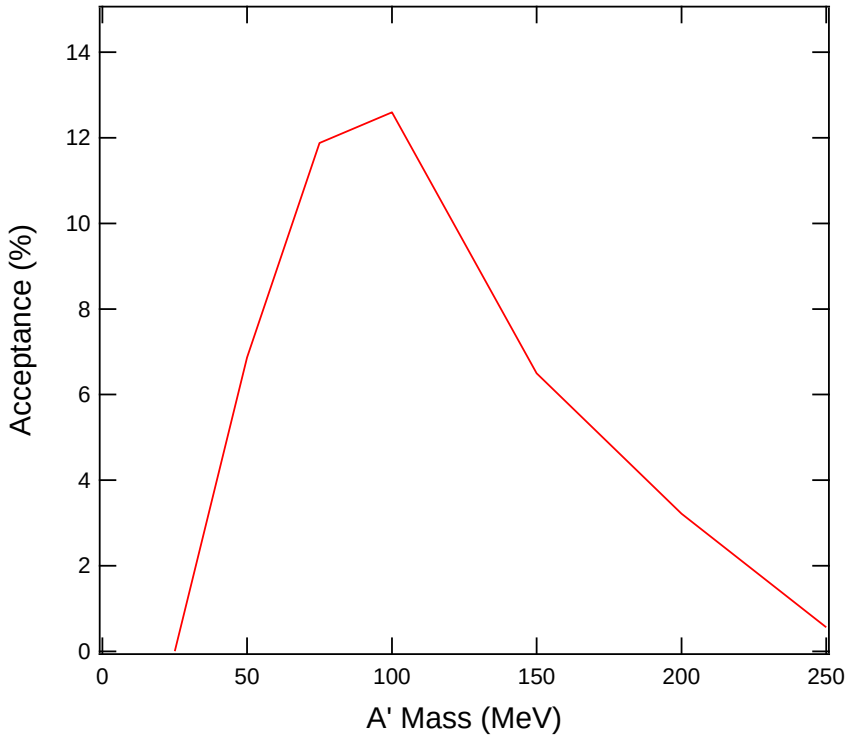

Figure 3.2.3 Tracker acceptance as a function of A′ mass.

3.3 **Tracking Performance**

We use a GEANT4 Si tracker simulation based on SLAC's org.lcsim infrastructure for full simulation of the passage of charged and neutral particles through the target and tracker. It creates realistic energy deposits in the silicon microstrip detectors, accounts for dead material, accurately digitizes energy deposits into strip hits, creates clusters, and performs track finding and reconstruction. This simulation is used to get realistic estimates of tracking pattern recognition efficiencies and purities in the presence of all the expected electromagnetic backgrounds, and to evaluate momentum, invariant mass, and vertex resolution.

In order to study the tracking performance of the detector (described below), we use samples of A' events at a variety of energies and decay lengths. On top of each event, we overlay backgrounds produced by the passage of 2.2GeV/c^2 beam electrons equivalent to 200nA in 7.5ns on a 0.125% W target and a beamspot of Gaussian sigma of 20μm in the vertical direction and 200μm in the horizontal.

3.3.1 **Tracking Efficiency, Pattern Recognition and Fake Rates**

Due to the requirements imposed on the tracks, the efficiency for finding tracks in the geometric acceptance is not 1. The average track reconstruction efficiency is 98% and the bulk of the inefficiency comes from the cut on the total χ^2 of the track.

Of the reconstructed tracks, a small percentage include a hit that is not from the correct electron. These "bad" hits may be from one of the high energy beam electrons scattered from the target into the detector or from a lower energy secondary. The left plot of Figure 3.3.1.1 shows the number of bad hits/track for both the electron and positron from the A' decay. The number of tracks with 0 bad hits is >98% and the positrons are slightly cleaner since occupancy of the positron side of the detector is smaller. The right plot of Figure 3.3.1.1 shows the layer number of the bad hit. Hits in the first two layers are the most often mistaken, and they tend to be both incorrect. We'll show how these bad hits affect the track parameters in the next section.

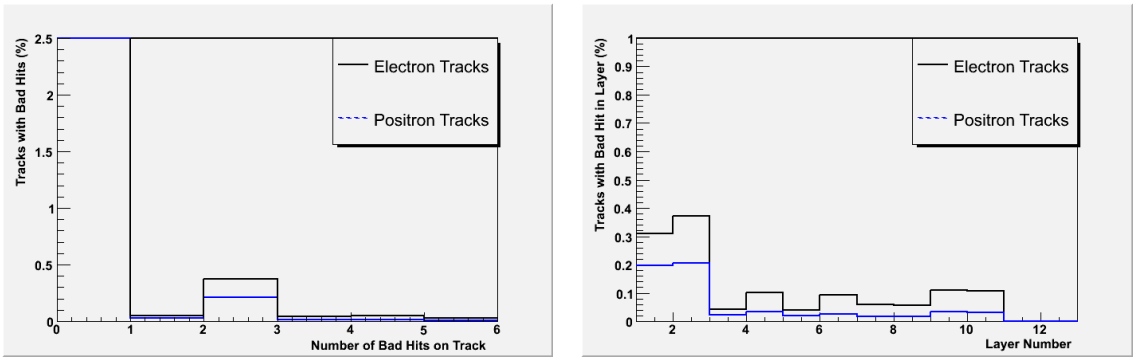

Figure 3.3.1.1: The number of bad hits (left) and the layer number of the bad hit (right) for electron (black) and positron (blue) tracks prior to vertex selection.

3.3.2 Track Momentum and Spatial Resolution

The momentum resolution is shown in Figure 3.3.2.1 as a function of momentum for tracks with 0 bad hits and for tracks with one or more. The momentum resolution for well-reconstructed tracks is σ_p/p = 4% while for hits with bad hits increases to 10%. This momemtum resolution is considerably worse than that in the full HPS proposal (~1.5%) because small angle stereo, which is used in the test run, provides much less precision in the bend plane than the 90 degree stereo which is used in full HPS. The lower resolution still provides adequate invariant mass resolution for this experiment.

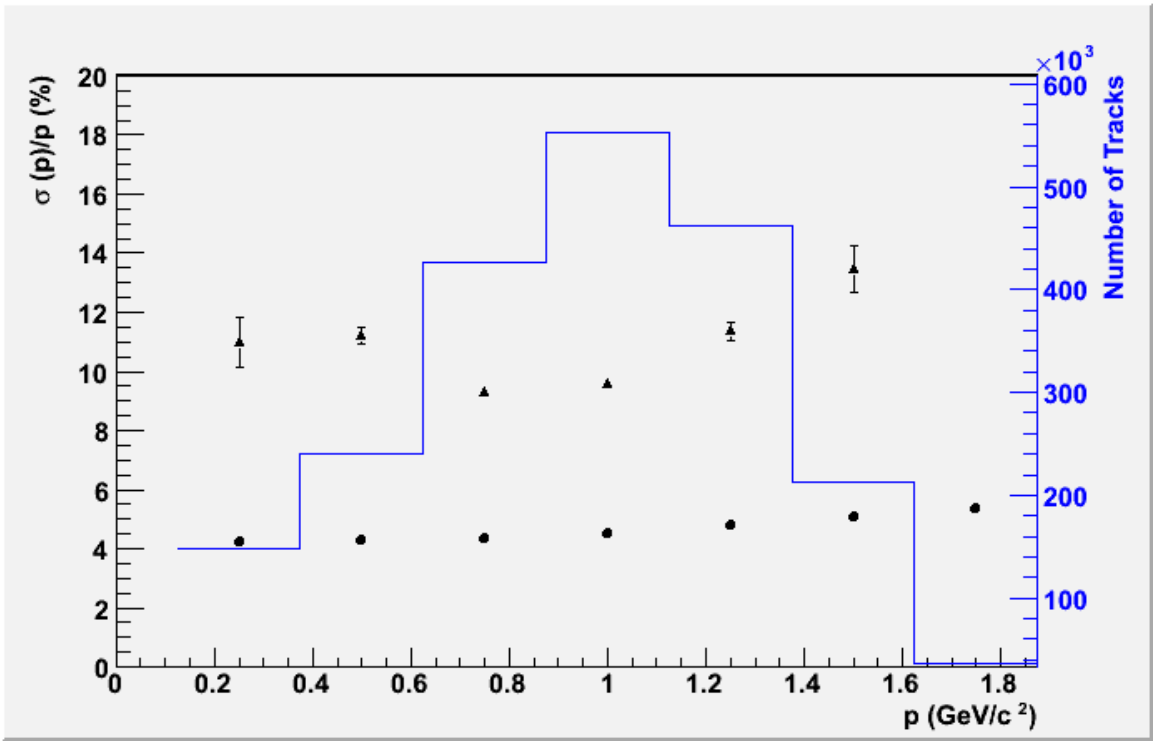

Figure 3.3.2.1: Fractional momentum resolution versus momentum for 0 bad hit tracks (circles) and tracks with 1 or more bad hits (triangles).

One quantity we use to determine track quality is the distance of closest approach (DOCA) to the beam axis. We use this instead of the DOCA to the target beam spot since we are interested in long-lived decays and tracks from those will not point back to the target. We separate the distance into the bend plane (XOCA) and non-bend plane (YOCA) distances. Below, in Figure 3.3.2.2, is the resolution of these quantities as function of momentum for tracks with 0 bad hits. The resolution is, on average, about 100μm (400 μm) in the non-bend (bend) direction but increases significantly at low momentum. The position resolution for tracks with one or more bad hits is somewhat worse, depending on which layer the bad hit is. In particular, when the bad hit is in the first non-bend layer (layer 1), the YOCA is very poorly determined as shown in

Figure 3.3.2.2. Tracks with bad hits in layers 1 or 2 are a major contribution to the tail of the vertex position distribution.

For long lived A′ decays, the position of the decay vertex is an important discriminating variable. The dominant background to A′ production is radiative events which originate in the target. Distinguishing A′ decays from the background therefore depends on the vertex resolution and in particular on the tails of the vertex distribution. In order to study the tails, we use large samples of A′ events decaying promptly overlaid on top of the simulated beam background events.

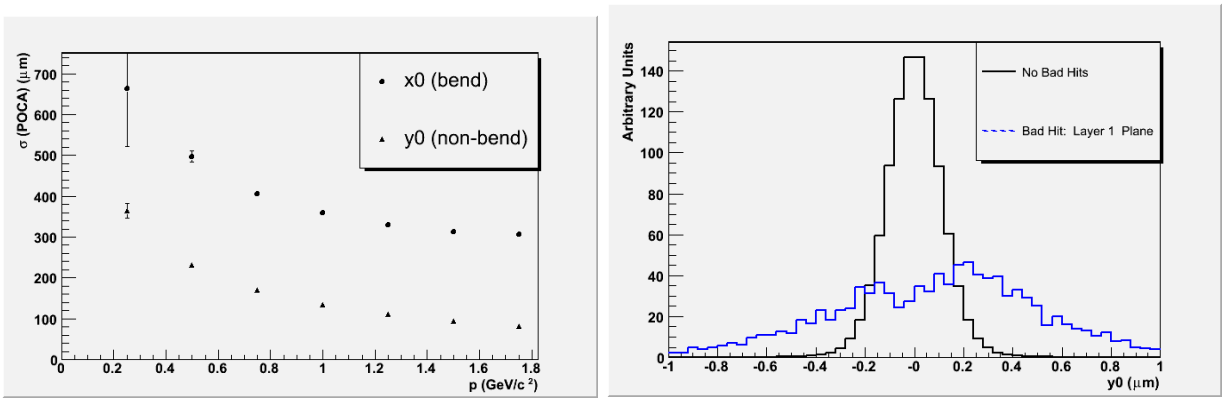

Figure 3.3.2.2: LEFT: The resolution of the position of closest approach to the beam axis versus track momentum. RIGHT: The YOCA resolution for tracks with 0 bad hits (black) and with a bad hit in layer 1 (blue).

Each pair of oppositely charged tracks is fit to a common vertex using a Kalman filtering method first suggested by Billoir [1,2] and used in many experiments. The method uses the measured helix parameters and their correlations to determine the most likely decay position of the A′ and also returns fitted momenta for each particle. We actually fit each pair twice with different hypotheses of their origin. We constrain either the vertex to be consistent with an A′:

- which originates in the 200μmx20μm beamspot at the target, and moves off in the direction given by the measured A′ momentum. This fit will be used for the vertexing search.

- which originates and decays at the target within the 200μmx20μm beamspot. This fit will be used for the bump-hunt only search.

For each electron/positron pair reconstructed in the tracker, we compute the invariant mass based on the fitted momenta of the tracks. The mass resolution depends on the invariant mass of the pair and is shown in Figure 3.3.2.3. The right-hand plot in Figure 3.3.2.3 shows the improvement in the resolution for the second fit, where the decay is assumed to occur in the target.

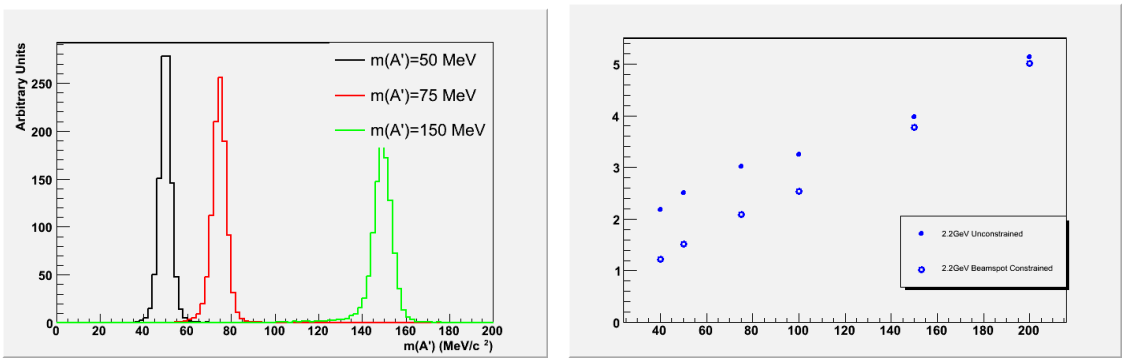

Figure 3.3.2.3 Left: The mass distributions for different generated A' masses. Right: The gaussian width of the mass distributions (MeV/c^2) vs generated A' mass (MeV/c^2). The open circles are the resolutions when the decay is constrained to the target beamspot and the closed circles are without this constraint.

Even for prompt decays, the z vertex position (V_z) distribution of all reconstructed e+e− pairs (solid black histogram, Figure 3.3.2.4) shows a long tail, still significant beyond 5cm. This tail is primarily comprised of events where one or both of the tracks use one or more bad hits. Fortunately there are a number of quantities we can use to minimize the tails. Namely, for purposes of this proposal, we make the following cuts:

- The χ^2 of each track is less than 20
- The total momentum of the A' candidate is less than the beam energy
- A very loose cut on the reconstructed vertex position $|V_x|<400\mu m$ and $|V_y|<400\ \mu m$
- The clusters in layer 1 of each track must be isolated from the next closest cluster by at least 500 μm
- A χ^2 cut on the vertex fit of less than 15

The vertex resolution depends on the invariant mass of the particles being vertexed. Lower masses have worse Gaussian resolutions as shown in Figure 3.3.2.4. This is expected since the error on the opening angle (θ), due to multiple scattering, scales like: $\sigma(\theta)/\theta \sim (1/E)/(m/E) \sim 1/m$.

Figure 3.3.2.5 shows the vertex resolution for samples of 40 MeV and 80 MeV A' events. The cuts above remove almost all of the tail past ~1.5cm (points with errors in Figure 3.3.2.5) while retaining ~50% of the e^+e^- pairs from the A' candidate. The events on the tail are enhanced with vertices where there are one or more bad hits on the track (represented by the blue histogram in Figure 3.3.2.5), although there is still a contribution from well-reconstructed tracks. The rejection of tracks with bad hits depends strongly on the precision of the virtual A' trajectory, which in turn depends on the size of the beamspot. Having a beamspot significantly smaller than the intrinsic tracker resolution, 100μm in the non-bend and 300 μm in the bend directions, is important.

In practice, there is much more we can do to clean up the vertex and mass resolution both at the track level (e.g. remove hits that are clearly from scattered beam electrons) and at the vertex level. These will be pursued in the near future.

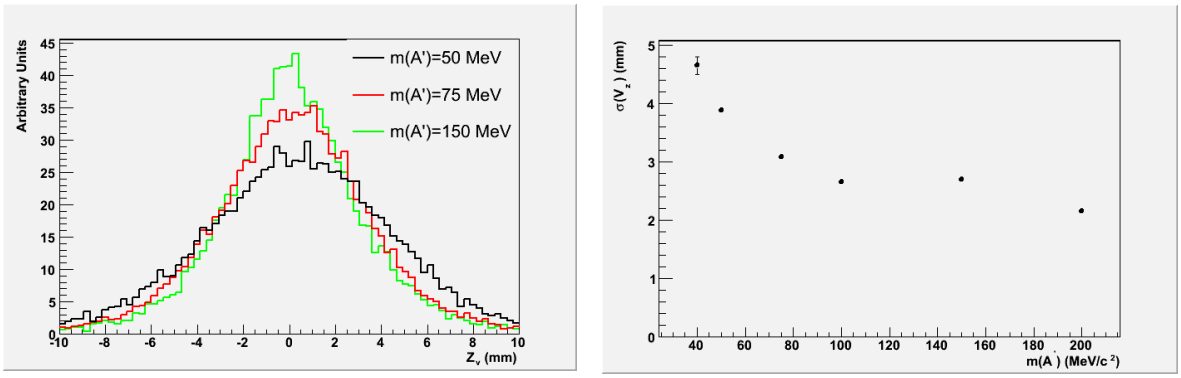

Figure 3.3.2.4 Left: The distribution of reconstructed vertex positions for A' different masses. Right: The (Gaussian) resolution dependence versus A' mass for signal-only events.

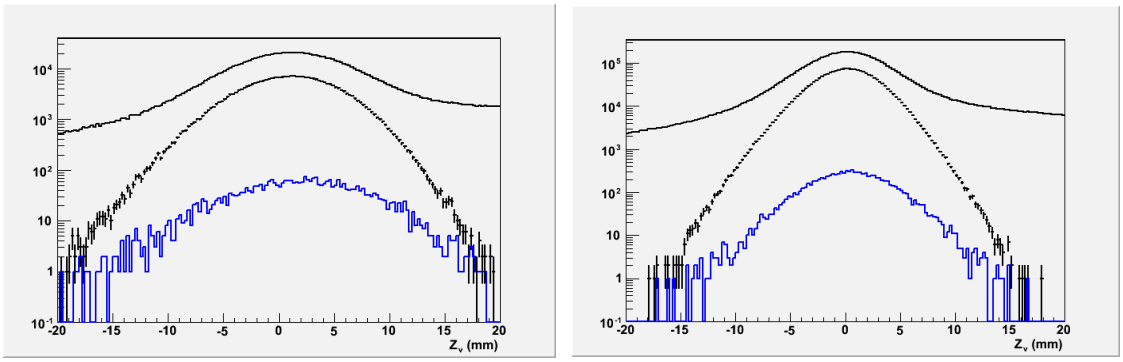

Figure 3.3.2.5: Distribution of the reconstructed vertex position along the beam axis for 2.2GeV 40MeV (left) and 80MeV (right) A' events before (solid black) and after (points with errors) selection. The blue histogram shows the distribution for pairs that have at least one bad hit after selection.

3.3.3 *References*

1. P. Billoir, R. Fruhwirth, and M. Regler, Nucl. Instr. And Meth. A241 (1985) 115.

2. P. Billoir and S. Qian, Nucl. Instr. And Meth. A311 (1991) 139.

4 Critical Outcomes

The HPS Test Run has a range of goals. The highest priority goals are those which validate the fundamental assumptions of the full HPS experiment and remove the contingencies for full HPS approval. There are two critical goals. One is verifying that the occupancies in the silicon vertex tracker are compatible with unambiguous track finding, accurate momentum measurement, and tail-free vertexing required for the full HPS. The other is that the trigger can operate with good efficiency and acceptance at rates below 50 kHz. Extensive Monte Carlo has demonstrated both these points in simulation; they need to be confirmed experimentally. There are a number of obvious prerequisites for establishing these two primary Test Run goals, involving the beam, the SVT apparatus, the ECal apparatus, and the respective data acquisition systems.

It is critical that we establish that the beam sizes, beam halo, and beam stability match the requirements of HPS at the proposed operating currents. First we must establish that the electron beam passes through the chicane, that the photon dump is properly positioned, and that the beam makes its way to the Hall B dump without excessive backgrounds in Hall B. The beam must be aligned to minimize backgrounds in the Ecal Vacuum chamber. Then we must measure beam sizes and beam halo, monitor short term beam stability, and develop beam turn-off procedures to protect against excessive beam motion. The target must be shown to survive the design beam currents with no ill effects.

The tracker must be capable of measuring the occupancies mentioned above. This requires we produce fully operational silicon sensors with front end readout for the whole tracker. Once the beam trajectory is established, the silicon sensors must be accurately positioned above and below it. The minimal requirement on the SVT DAQ is to readout the entire tracker given a random trigger and record the resulting data. This data, taken as a function of beam current and distance from the beam, will suffice for studies of silicon sensor occupancy.

The ECal must be aligned to a level that initial beam passage won't damage the $PbWO_4$ crystals. The crystals and readout chain must be operable and the ECAL DAQ must be able to read out the ECal at random times and record the resulting data. The environment of the crystals must be temperature controlled and stable. With the data taken for a variety of beam currents, we can study the energy depositions and occupancies in the crystals, and explore the trigger rates resulting from a variety of possible algorithms.

Beyond the most critical goals, we have additional objectives for the HPS Test Run. They depend on first meeting the goals mentioned above, and on establishing operating conditions that are conducive to taking good data.

Given acceptably low occupancies in the silicon vertex tracker, we will want to record random triggers for the sake of finding tracks and developing precision alignment procedures to determine the relative positions of all the layers. Background studies lead us to expect there to be several electron tracks scattered into the acceptance in each random trigger. These will allow us to study alignment accuracy, sensor efficiency, sensor noise, sensor resolution, and ultimately

track finding efficiency, momentum resolution, and vertex resolution. They will also let us study tracker time resolution and our ability to discriminate two pulses which overlap in time.

The next step with the ECal will involve commissioning the trigger. This will require successfully transferring ECal data to the trigger at high rate, reliable inter-crystal energy calibration, and the successful implementation of trigger algorithms. We will measure trigger rates as a function of beam current and target thickness, and compare the measurements to our offline predictions based on recording random triggers. Following trigger commissioning, we will implement the trigger in the overall DAQ.

After commissioning the trigger, the next step is to implement full rate, triggered data acquisition for both the SVT and the ECal. This can provide a sample of trident events, where many quantities can be studied: isolation of trident events from backgrounds, measurement of trident event kinematics and rates, mass distributions, and vertex resolution. It will also exercise the overall data acquisition system, event monitoring software, and our data storage capacity.

Given all the above, and the ability to take and record data at rates comparable to those in the proposal, the HPS Test Run can embark on recording data of physics interest, with the potential to establish new limits on heavy photon production. Figure 4.1 illustrates the expected reach for the proposed test run assuming 0.5×10^6s of beamtime (~1 week), shown as the blue curves. Also shown in red is the reach expected for the full run: two 9×10^6s run periods, one with 6.6 GeV beam energy and 450 nA on a 0.25% X_0 target and the other with 2.2 GeV 200 nA on a 0.125% X_0 target. The upper solid curves are the lower-limits of 2σ sensitivity for the full resonance search, while the lower solid contours are the outer limit of sensitivity for the vertex-based resonance search, corresponding to 2.4 events in a resolution-limited mass window, where the vertex requirement has been chosen so that 0.5 background events are expected. The dashed curves correspond to the 5σ sensitivities of the full run. The region accessible to the test run apparatus includes a region of parameter space suggested by ascribing the discrepancy between theoretical and experimental values of the muon anomalous magnetic moment to the existence of a heavy photon. See also Figure 1.1 in the Introduction.

In the event that the HPS Test Run cannot complete its entire program in Spring 2012 before the shutdown for the CEBAF Upgrade, we will assess how valuable a second data taking run aimed at reaching physics goals would be in the beginning of the 12 GeV Era, and how this would interact with preparing the full HPS experiment.

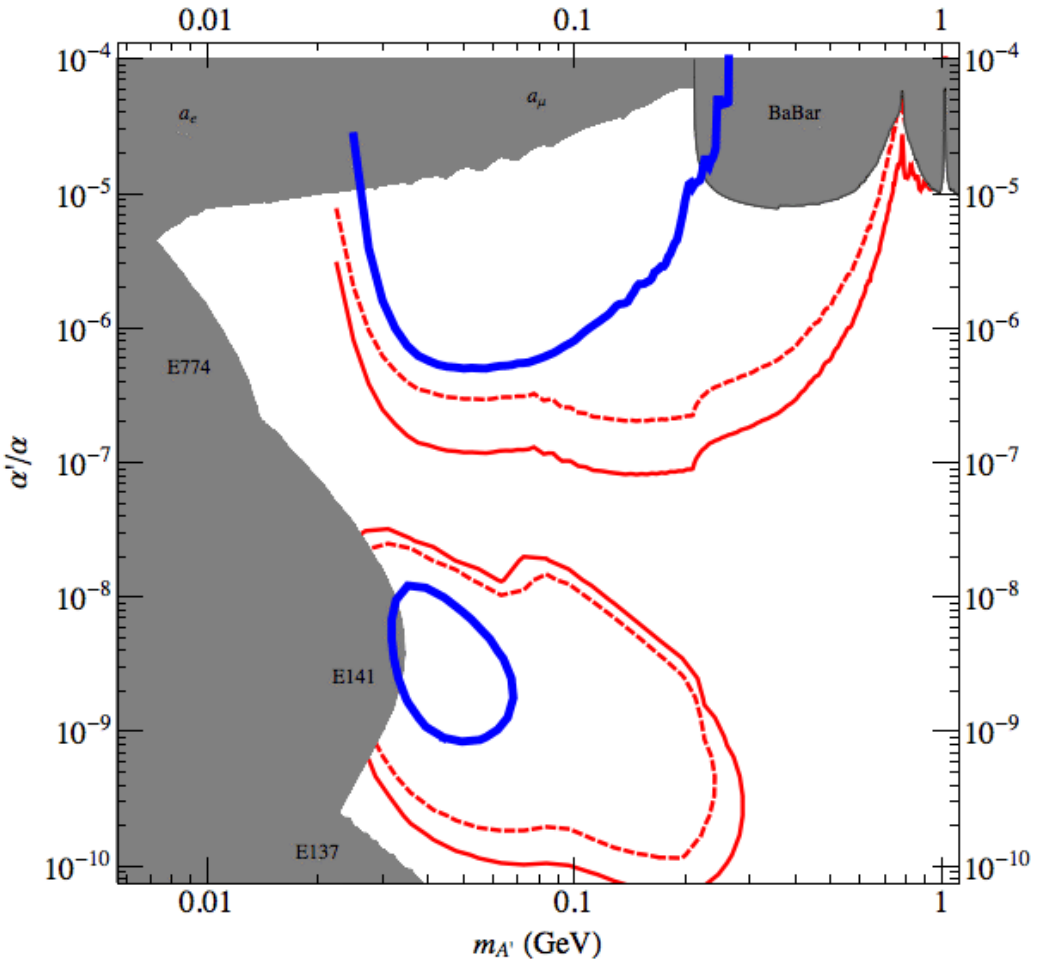

Figure 4.1 Anticipated reach in α'/α for the Heavy Photon Search (HPS) experiment, with existing constraints. The solid (dashed) red curves show the 2σ (5σ) sensitivity of the full experiment and the blue shows the 2σ sensitivity for the test run with 0.5×10^6s of beamtime.

5 Costs, Schedule and Manpower

Cost estimates for engineering, designing, fabricating, assembling, testing, and installing the Heavy Photon Search Test Run are given below. The costs reflect considerable savings coming from the donation of the silicon microstrip sensors from Fermilab, the use of some DAQ crates and equipment from SLAC, and many contributions from JLab, including $PbWO_4$ calorimeter crystals, the chicane and analyzing magnets, magnet power supplies, and beam diagnostic apparatus. Much of the calorimeter readout electronics utilizes designs which are already in place for the Hall B 12 GeV upgrade, eliminating engineering and design expense. Very significant cost savings come from utilizing the FADCs and data acquisition system being developed for the upgraded CLAS12 detector, which will be available to the Test Run. The Orsay group is providing engineering and design efforts for the ECal and its vacuum chamber, affording additional savings.

The costs are given in an accompanying WBS summary table, below, which itemizes the major items subsystem by subsystem, and indicates whether JLab (J) or SLAC (S) takes responsibility for construction. Engineering, design, and technician labor rates include lab overheads, and differ between the two laboratories. Contingencies have been set at 30% for labor and 35% for M&S at SLAC, and somewhat lower at JLab, since full engineering designs are not yet available for the SLAC items, and many of the JLab items are similar to items recently constructed. The contingency for commercial items is generally about 10%. Overheads have not been applied to M&S at either laboratory. Our DAQ and beamline cost estimates have been made by engineering groups at SLAC and JLab which are experienced in cost estimation and actively involved in many related projects. The SVT estimates came from physicists and engineers on the project, with experience in designing and fabricating silicon detector systems. The Ecal estimates come from physicists and engineers at JLab who have constructed a similar system, the CLAS IC, in the recent past.

The schedule for the overall project is included in a Project Summary table below. A brief description of the schedule for the different subsystems is also given. The overall schedule contingency is about 10%, and depends critically on the assumption that funding is available rapidly.

5.1 HPS Test Run Costs

Beamline expenses for the Test Run are held to a minimum by using the 18D36 magnet currently installed in Hall B as the analyzing magnet and two JLab Frascati chicane magnets. Some overall engineering and design will be required, beam pipes fabricated, the ecal vacuum chamber constructed, modifications made to the analyzing magnet vacuum chamber flanges and vacuum feedthroughs, a vacuum chamber built for the downstream Frascati magnet, and an existing photon dump and shielding inserted behind the second chicane magnet. A thin target must be built as well. Total beamline expenses are about $138k.

Testing occupancies in the silicon tracker requires development and construction of prototype sensor modules, the sensor module support system capable of moving sensors vertically, and power supplies and monitoring. SVT Electronics and DAQ are also needed and are costed below. The tracker/vertexer for the test run will cost about $168k.

The SVT readout requires hybrid and readout board engineering and prototyping, APV25 and chip procurement, fabrication, and test. The SVT DAQ also requires designing and prototyping the Trigger Interrupt ACTA card. SLAC will provide the ATCA crate, CPU, CIM, and Server. These components permit tests of the entire triggering chain and commissioning of the high rate data acquisition system. The expenses are dominated by engineering development, and total $200k.

JLab will donate the PbWO4 crystals used in the electromagnetic calorimeter. Orsay will donate engineering and design for a new enclosure for the crystals, but Jlab will need to fabricate the enclosure, the crystal support structure, the readout motherboard and connection board, and support fixtures. The total expense will be roughly $175k, including fabrication, assembly, and test. Reconfiguring the ecal is critical to HPS, to provide tests of the triggering rate and occupancies, and to allow beam transport in vacuum. The Test Run Ecal enclosure will serve for the full HPS experiment as well.

Trigger and DAQ electronics for the ECAL are being developed for the CLAS upgrade, so relatively little engineering and technician time will be needed in preparation of the HPS Test Run. Components, including the 250 MHz FADC boards, will be provided at no cost since they can be borrowed from the CLAS upgrade. The system test expenses will also be borne by JLab Hall B. The remaining costs total $32k.

Installation expenses are not included in the WBS because they will be borne by Jefferson Laboratory, utilizing the Hall B crew.

Travel and lodging expenses for SLAC trips to JLab are also included in this proposal. During design and construction, there will be a small number of trips to solidify and review designs, and to work together to begin DAQ integration of the SLAC and JLab systems. Funds are reserved for a collaboration meeting to be held sometime during calendar 2011. The bulk of the funds are reserved for installation, commissioning, and data taking for the test run. The total is $38k.

Altogether the Test Run will cost $751k. The test will provide invaluable experience with beam control issues, and measure the background and trigger rates for the HPS experiment. The test run will also test tracker and ECal prototypes, shakedown the proposed high rate readouts for both the SVT and Ecal, and provide an invaluable opportunity to integrate and debug the DAQ.

Item	Cost($k)
Beamline	138
Si Tracker	168
ECal	175
SVT DAQ	200
ECal Trigger/DAQ	32
Travel	38
TOTAL	**751**

5.2 Schedule

Our goal is to be ready to install the HPS Test Run by March, 2012, and proceed with installation, commissioning, and data taking during late Spring 2012, before the down for the 12 GeV Upgrade. This will require approval and funding for the Test Run as soon as possible. Schedules for each of the major subsystems of the experiment are attached below, and summarized here. Preparing for the test run in less than a year's time will be challenging, but possible. The schedule contingency is about 10%.

Work on the beamline engineering will commence when funding is secured. Engineering and design will proceed at the beginning of Quarter 2 of 2011 and conclude mid-Quarter 3. Fabrication of the beampipes, ecal vacuum chamber, the vacuum chamber for the downstream Frascati magnet, and modifications to the analyzing magnet vacuum chamber will begin mid Quarter 3. Fabrication will be completed in Quarter 4. Installation of the SVT and target in the analyzing magnet vacuum box begins in Quarter 4, and is completed mid-Quarter 1, 2012.

The SVT engineering and design begins in earnest at the beginning of Quarter 2, first on the sensor modules, and then on the support structure. Assembly of the sensor modules will follow production and test of the hybrids (see SVT DAQ below) and the CF supports and begin in Quarter 3. The support structure will be fabricated in the same time frame. Assembly of the modules on the support structure begins in quarter 4. Preparation of power supplies, cables, and the cooling and motion systems will proceed in quarters 3 and 4, with full assembly and test of the tracker coming by the end of quarter 4, followed by installation into the analyzing magnet vacuum chamber.

The ECal engineering design effort commences in Quarter 2 of 2011, and will be completed near the beginning of Quarter 3. Fabrication of the ECal enclosure, crystal support system, and electronics boards begins in Quarter 3 and will extend to mid Quarter 4. Assembly and test begin Quarter 4 and finish mid Quarter 1, 2012.

The SVT DAQ system is already in design, and design of its several components will be completed serially, finishing mid Quarter 2. Firmware and software development will proceed through this same period. Hybrid fabrication begins mid Quarter 2, followed by RTM and COB-DTM fabrication. When complete and tested, hybrids will be wire bonded to sensor modules,

and the sensors tested with the full DAQ chain. The DAQ system integration and testing begins during Quarter 3 and proceeds to the end of Quarter 4. Integration of the SVT DAQ with the JLab DAQ begins mid Quarter 4, and is completed by mid-Quarter 1 of 2012.

The ECal DAQ proceeds with the fabrication of existing designs. FADC boards, the Crate Trigger Processor, the Trigger Interface Board, and the Sub-System processor Boards will all be fabricated during Quarter 2 of 2011. Assembly and test of a full crate of FADCs begins in late Quarter 2 and extends to the beginning of Quarter 4. Fabrication of modules for the second crate will be completed in Quarter 4, and the entire Ecal System tested at the end of Quarter 4. Integration with the SVT electronics begins in mid Quarter 4, extending into Quarter 1 of 2012.

Installation will begin nominally in Quarter 2 of 2012, contingent on the Jefferson Laboratory schedule.

5.3 **Manpower**

The manpower needed to design, fabricate, assemble, test, install, and commission the HPS Test Run is captured in the WBS tables. The HPS Collaboration has the personnel needed to realize this project.

Beamline design work will be done at JLab by Arne Freyberger and Stepan Stepanyan and at SLAC by Ken Moffeit, engineering at SLAC by Marco Oriunno, Dieter Walz, and Clive Field, fabrication in the JLab shops, and installation by the Hall B crew. Engineering for the Ecal vacuum chamber is being done by Philippe Rosier at Orsay in consultation with Marco Oriunno. Beam diagnostics and slow control will be supported by Nerses Gevorgyan (Yerevan) and Hovanes Egiyan.

The Tracker/Vertexer will be engineered and designed by Marco Oriunno, Tim Nelson, and Rich Partridge, with additional help from Bill Cooper and Alex Grillo, all experienced with silicon detector systems. Others at SLAC and UCSC will help with test and assembly, including Matt Graham, Takashi Maruyama, John Jaros, V. Fadeyev, a post doc, and graduate students. Jim MacDonald will serve as technician at SLAC. Work will be closely coordinated with Gunther Haller's Electronics group at SLAC (see below).

The Ecal is being designed by the Orsay Group, especially Philippe Rosier, Emmanuel Rindel, Emmanuel Rauly, and Michel Guidal, with participation by the Jlab group, especially Stepan Stepanyan, F.-X. Girod and Alex Koubarovski (RPI). Others at JLab and in the collaboration will help in assembly and test of the ECal, especially groups from the Collage of William and Mary (Keith Griffioen), Norfolk State University (Carlos Salgado), and INFN Genova(Italy).

The SVT DAQ is being done by Haller's group at SLAC, including Gunther Haller, Ryan Herbst, Tung Phan, Bruce Klein, and Raghuveer Ausoori. Physicists Rich Partridge, Alex Grillo, and

Tim Nelson will collaborate closely. Postdocs and students will help debug, test, and certify DAQ electronics.

The Ecal Trigger/DAQ work is done in Sergey Boiarinov's group, which supports Hall B activities. H. Egiyan, F.-X. Girod, and V. Kubarovsky will collaborate with this group in assembling and testing the electronics, programming the trigger, and integrating it with the Ecal hardware.

The HPS collaboration is nearly 60 strong, so has adequate manpower for overall installation, commissioning, and data taking.

Simulation work is supported by Maurik Holtrop, Richard Partridge, Matt Graham, Ungaro (UCON), and Takashi Maruyama, along with help from students and Norman Graf at SLAC. Data management and storage and computing infrastructure will be overseen by Sergey Boiarinov and Maurik Holtrop and Homer Neal, all very experienced professionals. Analysis and simulation studies have been initiated by Maurik Holtrop, Matt Graham, Richard Partridge, and Takashi Maruyama. Students are actively being engaged.

The HPS collaboration is managed by its three spokespersons, Maurik Holtrop, John Jaros, and Stepan Stepanyan.

WBS	Component	Number	Unit	Materials	MContingency	Labor	LContingency	MTotal	LTotal	Total	Comment
1	Heavy Photon Search	1	each	390,500	98,800	204,115	57,995	489,300	262,110	751,410	
1.1	Test Run Experiment	1	each	390,500	98,800	204,115	57,995	489,300	262,110	751,410	
1.1.1	Test Run Beamline (J)	1	each	75,500	20,525	32,475	9,327	96,025	41,802	137,827	
1.1.1.1	Mechanical Engineer(J)	20	man hour	0	0	88	18	0	2,112	2,112	
1.1.1.2	Mechanical Designer(J)	40	man hour	0	0	60	12	0	2,880	2,880	
1.1.1.3	Analyzing Magnet	1	each	0	0	0	0	0	0	0	Jlab provides
1.1.1.4	Chicane Dipoles (J)	2	each	0	0	0	0	0	0	0	Jlab provides
1.1.1.5	Magnet Power Supplies (J)	2	each	0	0	0	0	0	0	0	Jlab provides
1.1.1.6	Test Run Beam Pipe	1	lot	4,000	1,000	0	0	5,000	0	5,000	
1.1.1.7	Test Run Target(S)	1	each	7,500	2,625	0	0	10,125	0	10,125	
1.1.1.8	Test Run Photon Dump	1	each	0	0	0	0	0	0	0	Jlab provides
1.1.1.9	Test Run Shielding	1	each	0	0	0	0	0	0	0	Jlab provides
1.1.1.10	ECal Vacuum Chamber	1	each	40,000	10,000	0	0	50,000	0	50,000	
1.1.1.10.1	Mechanical engineer(O)	80	man hour	0	0	0	0	0	0	0	Orsay provides
1.1.1.10.2	Ecal Vac Chamber Fab(J)	1	each	40,000	10,000	0	0	50,000	0	50,000	
1.1.1.11	Modify Magnet Vac Chamber	1	each	14,000	4,400	20,740	6,222	18,400	26,962	45,362	
1.1.1.11.1	Mechanical Engineer(S)	60	man hour	0	0	175	53	0	13,650	13,650	
1.1.1.11.2	Mechanical Technician(S)	80	man hour	0	0	128	38	0	13,312	13,312	
1.1.1.11.3	Vac Chamber Flange(J)	1	lot	5,000	1,250	0	0	6,250	0	6,250	
1.1.1.11.4	Test Vac Chamber M&S	1	each	9,000	3,150	0	0	12,150	0	12,150	
1.1.1.12	Frascati Magnet Vac Chamber	1	each	10,000	2,500	7,575	2,273	12,500	9,848	22,348	
1.1.1.12.1	Mechanical Engineer(S)	25	man hour	0	0	175	53	0	5,688	5,688	
1.1.1.12.2	Mechanical Technician(S)	25	man hour	0	0	128	38	0	4,160	4,160	
1.1.1.12.3	Vac Box and Flange(J)	1	lot	10,000	2,500	0	0	12,500	0	12,500	
1.1.2	Test Run Tracker (S)	1	each	48,000	16,300	79,880	23,964	64,300	103,844	168,144	
1.1.2.1	Sensor Modules for test	1	each	13,000	4,550	37,120	11,136	17,550	48,256	65,806	
1.1.2.1.1	Test Sensor Module M&S	1	lot	13,000	4,550	0	0	17,550	0	17,550	
1.1.2.1.2	Si Microstrip Sensors	25	each	0	0	0	0	0	0	0	Fermilab provides
1.1.2.1.3	SLAC ME	340	man hour	0	0	0	0	0	0	0	SLAC provides
1.1.2.1.4	Mechanical Technician(S)	290	man hour	0	0	128	38	0	48,256	48,256	
1.1.2.1.5	Graduate Student	220	man hour	0	0	0	0	0	0	0	SLAC provides
1.1.2.1.6	Physicist	160	man hour	0	0	0	0	0	0	0	SLAC provides
1.1.2.2	Module Support for Test	1	each	17,000	5,950	35,760	10,728	22,950	46,488	69,438	
1.1.2.2.1	Test Support Box M&S	1	lot	17,000	5,950	0	0	22,950	0	22,950	
1.1.2.2.2	Mechanical Engineer(S)	80	man hour	0	0	175	53	0	18,200	18,200	
1.1.2.2.3	Mechanical Technician(S)	170	man hour	0	0	128	38	0	28,288	28,288	
1.1.2.3	Power and Temp Systems for Test	1	each	18,000	5,800	0	0	23,800	0	23,800	
1.1.2.3.1	LV Power supplies for Test	0	lot	0	0	0	0	0	0	0	SLAC provides
1.1.2.3.2	HV Power supplies for Test	0	each	0	0	0	0	0	0	0	SLAC provides
1.1.2.3.3	LV and HV Cables for Test	1	lot	3,000	1,050	0	0	4,050	0	4,050	
1.1.2.3.4	Chiller for Test	1	each	5,000	1,250	0	0	6,250	0	6,250	
1.1.2.3.5	Si System Monitoring	1	lot	10,000	3,500	0	0	13,500	0	13,500	
1.1.2.4	Install and Test	1	each	0	0	7,000	2,100	0	9,100	9,100	
1.1.2.4.1	Mechanical Engineer(S)	40	man hour	0	0	175	53	0	9,100	9,100	
1.1.2.4.2	Physicist	160	man hour	0	0	0	0	0	0	0	SLAC provides

WBS	Component	Number	Unit	Materials	MContingency	Labor	LContingency	MTotal	LTotal	Total	Comment
1.1.2.4.3	Graduate Student	140	man hour	0	0	0		0	0	0	SLAC provides
1.1.3	Test Run Ecal (J)	1	each	130,000	32,500	10,600	2,120	162,500	12,720	175,220	
1.1.3.1	Ecal Enclosure	1	each	80,000	20,000	0	0	100,000	0	100,000	
1.1.3.1.1	Mechanical engineer(O)	80	man hour	0	0	0	0	0	0	0	Orsay provides
1.1.3.1.2	Fab Ecal Enclosure	1	each	80,000	20,000	0	0	100,000	0	100,000	
1.1.3.2	Crystal Support Structure	1	each	20,000	5,000	0	0	25,000	0	25,000	
1.1.3.2.1	Mechanical engineer(O)	40	man hour	0	0	0	0	0	0	0	Orsay provides
1.1.3.2.2	Fab Crystal Support	1	each	20,000	5,000	0	0	25,000	0	25,000	
1.1.3.3	Connection Board	1	each	7,000	1,750	0	0	8,750	0	8,750	
1.1.3.3.1	Electronic Engineer(O)	40	man hour	0	0	0	0	0	0	0	Orsay provides
1.1.3.3.2	PbWO4 Connection Board	1	each	7,000	1,750	0	0	8,750	0	8,750	
1.1.3.4	Motherboard	1	each	13,000	3,250	0	0	16,250	0	16,250	
1.1.3.4.1	Electronic Engineer(O)	40	man year	0	0	0	0	0	0	0	Orsay provides
1.1.3.4.2	PbWO4 Motherboard	1	each	13,000	3,250	0	0	16,250	0	16,250	
1.1.3.5	Support Stand	1	each	10,000	2,500	0	0	12,500	0	12,500	
1.1.3.6	Test and Select Modules	1	each	0	0	0	0	0	0	0	
1.1.3.6.1	Graduate Student	80	man hour	0	0	0	0	0	0	0	Collaboration
1.1.3.6.2	Physicist	80	man hour	0	0	0	0	0	0	0	Collaboration
1.1.3.7	Assemble Ecal	1	each	0	0	10,600	2,120	0	12,720	12,720	
1.1.3.7.1	Mechanical Technician(J)	200	man hour	0	0	53	11	0	12,720	12,720	
1.1.3.8	Test and Calibrate ECal	1	each	0	0	0	0	0	0	0	
1.1.3.8.1	Graduate Student	80	man hour	0	0	0	0	0	0	0	Collaboration
1.1.3.8.2	Physicist	80	man hour	0	0	0	0	0	0	0	Collaboration
1.1.4	Test Run SVT DAQ (S)	1	each	92,500	25,025	63,520	19,056	117,525	82,576	200,101	
1.1.4.1	Hybrid for Test	1	each	18,000	5,700	0	0	23,700	0	23,700	
1.1.4.1.1	APV25 Readout Chip	120	each	25	4	0	0	3,450	0	3,450	
1.1.4.1.2	SLAC EE	20	man hour	0	0	0	0	0	0	0	
1.1.4.1.3	SLAC E Designer	80	man hour	0	0	0	0	0	0	0	SLAC provides
1.1.4.1.4	Hybrid Board Fab	30	each	500	175	0	0	20,250	0	20,250	
1.1.4.1.5	Hybrid Test	1	each	0	0	0	0	0	0	0	
1.1.4.1.5.1	SLAC E Tech	80	man hour	0	0	0	0	0	0	0	SLAC provides
1.1.4.2	Readout board for Test	1	each	69,000	18,525	4,780	1,434	87,525	6,214	93,739	
1.1.4.2.1	RTM- Hybrid	1	each	10,500	3,675	2,560	768	14,175	3,328	17,503	
1.1.4.2.1.1	SLAC E Designer	60	man hour	0	0	0	0	0	0	0	SLAC provides
1.1.4.2.1.2	RTM hybrid fab	7	each	1,500	525	0	0	14,175	0	14,175	
1.1.4.2.1.3	RTM test	1	each	0	0	2,560	768	0	3,328	3,328	
1.1.4.2.1.3.1	Mechanical Technician(S)	20	man hour	0	0	128	38	0	3,328	3,328	
1.1.4.2.2	COB with DTM	5	each	4,500	450	0	0	24,750	0	24,750	
1.1.4.2.3	COB-DPM	1	each	36,000	12,600	2,220	666	48,600	2,886	51,486	
1.1.4.2.3.1	SLAC EE	120	man hour	0	0	0	0	0	0	0	SLAC provides
1.1.4.2.3.2	SLAC E Designer	40	man hour	0	0	0	0	0	0	0	SLAC provides
1.1.4.2.3.3	COB DTM Fab	24	each	1,500	525	0	0	48,600	0	48,600	
1.1.4.2.3.4	COB DTM Test	1	each	0	0	2,220	666	0	2,886	2,886	
1.1.4.2.3.4.1	Electronic Technician(S)	20	man hour	0	0	111	33	0	2,886	2,886	
1.1.4.3	TI ACTA for Test	1	each	5,500	800	2,220	666	6,300	2,886	9,186	

Page 2 of 3

WBS	Component	Number	Unit	Materials	MContingency	Labor	LContingency	MTotal	LTotal	Total	Comment
1.1.4.3.1	RTM timing	1	each	1,000	350	2,220	666	1,350	2,886	4,236	
1.1.4.3.1.1	SLAC EE	20	man hour	0	0	0	0	0	0	0	SLAC provides
1.1.4.3.1.2	SLAC E Designer	40	man hour	0	0	0	0	0	0	0	SLAC provides
1.1.4.3.1.3	RTM timing Fab	1	each	1,000	350	0	0	1,350	0	1,350	
1.1.4.3.1.4	RTM timing test	1	each	0	0	2,220	666	0	2,886	2,886	
1.1.4.3.1.4.1	Electronic Technician(S)	20	man hour	0	0	111	33	0	2,886	2,886	
1.1.4.3.2	COB with DTM	1	each	4,500	450	0	0	4,950	0	4,950	
1.1.4.4	ATCA crate/CPU	1	each	0	0	0	0	0	0	0	
1.1.4.4.1	ATCA Crate/CPU M&S	1	lot	0	0	0	0	0	0	0	SLAC provides
1.1.4.5	System Integration	1	each	0	0	56,520	16,956	0	73,476	73,476	
1.1.4.5.1	Server	1	each	0	0	0	0	0	0	0	SLAC provides
1.1.4.5.2	Electronic Engineer(S)	360	man hour	0	0	157	47	0	73,476	73,476	
1.1.4.5.3	Physicist	160	man hour	0	0	0	0	0	0	0	
1.1.5	Test Ecal Trigger/DAQ	1	each	10,000	1,000	17,640	3,528	11,000	21,168	32,168	
1.1.5.1	Electronic Engineer(J)	80	man hour	0	0	88	18	0	8,448	8,448	
1.1.5.2	Electronic Technician(J)	200	man hour	0	0	53	11	0	12,720	12,720	
1.1.5.3	FADC Board	45	each	0	0	0	0	0	0	0	JLAB provides
1.1.5.4	TI Board	2	each	0	0	0	0	0	0	0	JLAB provides
1.1.5.5	SD Board	2	each	0	0	0	0	0	0	0	JLAB provides
1.1.5.6	SD Board	2	each	0	0	0	0	0	0	0	JLAB provides
1.1.5.7	CTP Board	2	each	0	0	0	0	0	0	0	JLAB provides
1.1.5.8	CPU Board	2	each	0	0	0	0	0	0	0	JLAB provides
1.1.5.9	VXS Crate	2	each	0	0	0	0	0	0	0	JLAB provides
1.1.5.10	Test Cal Cables	1	lot	10,000	1,000	0	0	11,000	0	11,000	
1.1.6	System (J)	1	each	0	0	0	0	0	0	0	
1.1.6.1	Network Switches/Routers	1	lot	0	0	0	0	0	0	0	JLAB provides
1.1.6.2	Event Builder	1	each	0	0	0	0	0	0	0	JLAB provides
1.1.6.3	File Server	1	each	0	0	0	0	0	0	0	JLAB provides
1.1.6.4	Event Recorder	1	each	0	0	0	0	0	0	0	JLAB provides
1.1.7	SLAC Travel	1	each	34,500	3,450	0	0	37,950	0	37,950	
1.1.7.1	Consultation at JLab	1	each	6,000	600	0	0	6,600	0	6,600	
1.1.7.1.1	Travel, food, lodging for 1 week	4	each	1,500	150	0	0	6,600	0	6,600	
1.1.7.2	Attend collaboration Meeting	1	each	7,500	750	0	0	8,250	0	8,250	
1.1.7.2.1	Travel, food, lodging for 1 week	5	each	1,500	150	0	0	8,250	0	8,250	
1.1.7.3	Install and Commission	1	each	15,000	1,500	0	0	16,500	0	16,500	
1.1.7.3.1	Travel, food, lodging for 1 week	10	each	1,500	150	0	0	16,500	0	16,500	
1.1.7.4	Data Run	1	each	6,000	600	0	0	6,600	0	6,600	
1.1.7.4.1	Travel, food, lodging for 1 week	4	each	1,500	150	0	0	6,600	0	6,600	

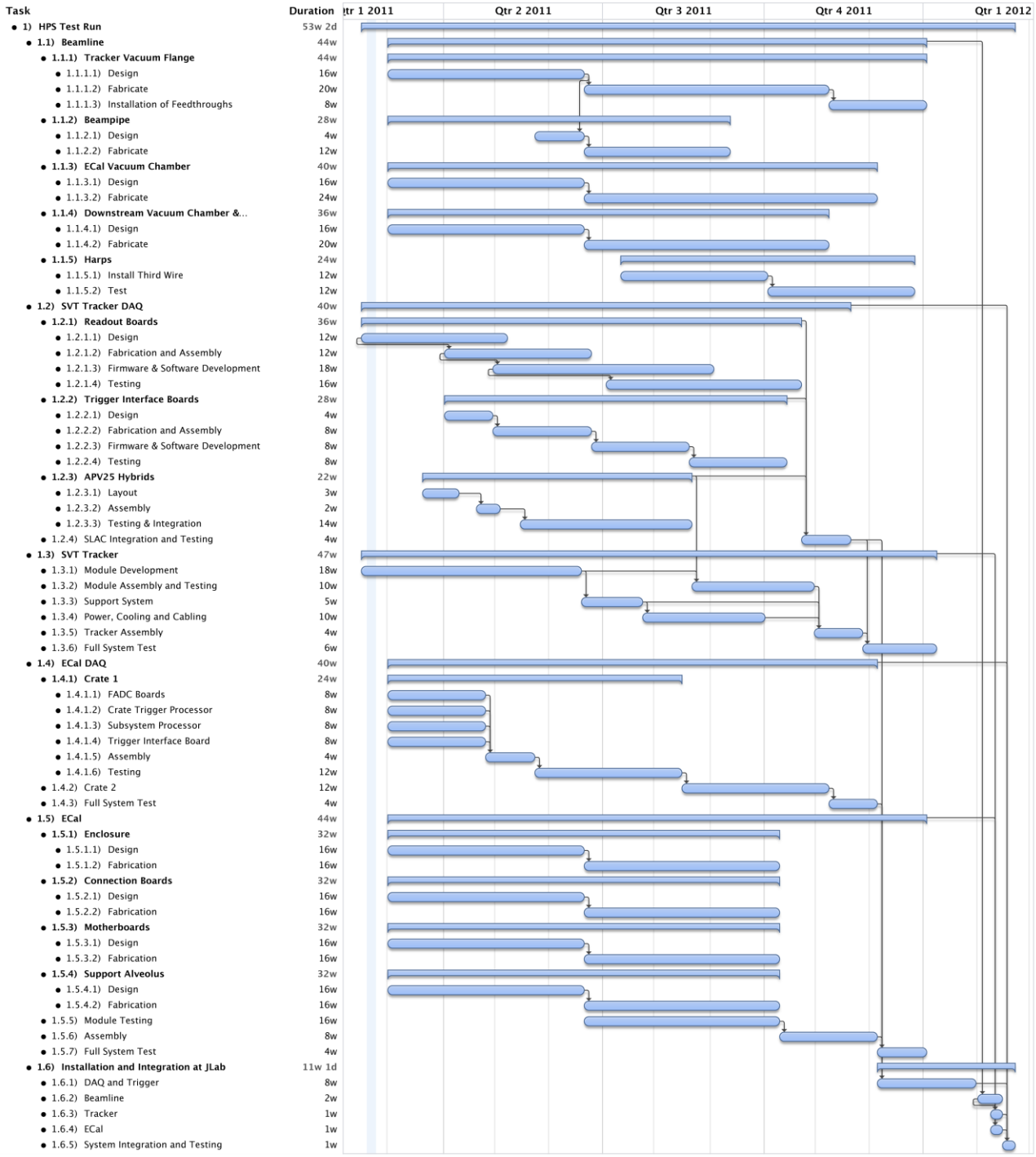
Task
Duration
tr 1 2011
Qtr 2 2011
Qtr 3 2011
Qtr 4 2011
Qtr 1 2012
1) HPS Test Run 53w 2d
1.1) Beamline 44w
1.1.1) Tracker Vacuum Flange 44w
1.1.1.1) Design 16w
1.1.1.2) Fabricate 20w
1.1.1.3) Installation of Feedthroughs 8w
1.1.2) Beampipe 28w
1.1.2.1) Design 4w
1.1.2.2) Fabricate 12w
1.1.3) ECal Vacuum Chamber 40w
1.1.3.1) Design 16w
1.1.3.2) Fabricate 24w
1.1.4) Downstream Vacuum Chamber &... 36w
1.1.4.1) Design 16w
1.1.4.2) Fabricate 20w
1.1.5) Harps 24w
1.1.5.1) Install Third Wire 12w
1.1.5.2) Test 12w
1.2) SVT Tracker DAQ 40w
1.2.1) Readout Boards 36w
1.2.1.1) Design 12w
1.2.1.2) Fabrication and Assembly 12w
1.2.1.3) Firmware & Software Development 18w
1.2.1.4) Testing 16w
1.2.2) Trigger Interface Boards 28w
1.2.2.1) Design 4w
1.2.2.2) Fabrication and Assembly 8w
1.2.2.3) Firmware & Software Development 8w
1.2.2.4) Testing 8w
1.2.3) APV25 Hybrids 22w
1.2.3.1) Layout 3w
1.2.3.2) Assembly 2w
1.2.3.3) Testing & Integration 14w
1.2.4) SLAC Integration and Testing 4w
1.3) SVT Tracker 47w
1.3.1) Module Development 18w
1.3.2) Module Assembly and Testing 10w
1.3.3) Support System 5w
1.3.4) Power, Cooling and Cabling 10w
1.3.5) Tracker Assembly 4w
1.3.6) Full System Test 6w
1.4) ECal DAQ 40w
1.4.1) Crate 1 24w
1.4.1.1) FADC Boards 8w
1.4.1.2) Crate Trigger Processor 8w
1.4.1.3) Subsystem Processor 8w
1.4.1.4) Trigger Interface Board 8w
1.4.1.5) Assembly 4w
1.4.1.6) Testing 12w
1.4.2) Crate 2 12w
1.4.3) Full System Test 4w
1.5) ECal 44w
1.5.1) Enclosure 32w
1.5.1.1) Design 16w
1.5.1.2) Fabrication 16w
1.5.2) Connection Boards 32w
1.5.2.1) Design 16w
1.5.2.2) Fabrication 16w
1.5.3) Motherboards 32w
1.5.3.1) Design 16w
1.5.3.2) Fabrication 16w
1.5.4) Support Alveolus 32w
1.5.4.1) Design 16w
1.5.4.2) Fabrication 16w
1.5.5) Module Testing 16w
1.5.6) Assembly 8w
1.5.7) Full System Test 4w
1.6) Installation and Integration at JLab 11w 1d
1.6.1) DAQ and Trigger 8w
1.6.2) Beamline 2w
1.6.3) Tracker 1w
1.6.4) ECal 1w
1.6.5) System Integration and Testing 1w